Regionally distinct trophoblast regulate barrier function and invasion in the human placenta

Bryan Marsh[1, 2, 3, 4], Yan Zhou[1, 3, 5], Mirhan Kapzidic[1, 3, 5], Susan Fisher[1, 3, 5*], and Robert Blelloch[1,2, 3*]

[1]The Eli and Edythe Broad Center of Regeneration Medicine and Stem Cell Research, University of California, San Francisco, San Francisco, CA 94143, USA
[2]Department of Urology, University of California, San Francisco, San Francisco, CA 94143, USA
[3]Center for Reproductive Sciences, University of California, San Francisco, San Francisco, CA 94143, USA
[4]Developmental and Stem Cell Biology Graduate Program, University of California, San Francisco, San Francisco, CA 94143, USA
[5]Department of Obstetrics, Gynecology, and Reproductive Sciences, University of California, San Francisco, San Francisco, CA 94143, USA
*Correspondence: robert.blelloch@ucsf.edu; susan.fisher@ucsf.edu

Abstract

The human placenta contains two specialized regions: the villous chorion where gases and nutrients are exchanged between maternal and fetal blood, and the smooth chorion which surrounds more than 70% of the developing fetus but whose cellular composition and function is poorly understood. Here, we use single cell RNA sequencing to compare the cell types and molecular programs between these two regions in the second trimester human placenta. Each region consists of progenitor cytotrophoblasts (CTBs) and extra-villous trophoblasts (EVTs) with similar gene expression programs. While CTBs in the villous chorion differentiate into syncytiotrophoblasts, they take an alternative trajectory in the smooth chorion producing a previously unknown CTB population which we term smooth-chorion-specific CTBs (SC-CTBs). Marked by expression of region-specific cytokeratins, the SC-CTBs form a stratified epithelium above a basal layer of progenitor CTBs. They express epidermal and metabolic transcriptional programs consistent with a primary role in defense against physical stress and pathogens. Additionally, we show that SC-CTBs closely associate with EVTs and secrete factors that inhibit the migration of the EVTs. This restriction of EVT migration is in striking contrast to the villous region where EVTs migrate away from the chorion and invade deeply into the decidua. Together, these findings add an important new dimension to our understanding of CTB differentiation in these distinct regions of the human placenta. This knowledge has broad implications for studies of the development, functions, and diseases of the human placenta.

Impact Statement

Single cell RNA-sequencing of distinct regions of the human placenta identifies a smooth chorion-specific cytotrophoblast population responsible for unique functions of the smooth chorion, including acting as a barrier and restricting invasion.

Introduction

The human placenta is the first organ to develop and forms the essential bridge between maternal and fetal tissues beginning at implantation (Knöfler et al., 2019; Turco and Moffett, 2019). The placenta must develop rapidly upon conception as it performs myriad functions that remain rudimentary in the developing embryo/fetus such as nutrient and oxygen transport and protection from mechanical and pathogenic insults. The placental also performs unique functions such as modulation of maternal tolerance and hormone production (Maltepe and Fisher, 2015;

Knöfler et al., 2019; Turco and Moffett, 2019). Beginning at implantation, placental development proceeds asymmetrically to produce two distinct regions. At the human implantation site, the embryonic pole, trophectoderm and associated mesoderm cells give rise to the villous chorion including the placental villi and basal plate, which are essential for the exchange of gases and nutrients. The chorionic villi that arise from the opposite side, the abembyronic pole, undergo a cycle of generation and degeneration eventually forming the smooth chorion, which fuses with the amnion and constitutes the fetal membranes. (Hamilton and Boyd, 1960; Boyd and Hamilton, 1967; Benirshcke et al., 2006). Compared to the villous chorion, little effort has been made to analyze types and functions of the CTBs that comprise the smooth chorion (Benirshcke et al., 2006, Garrido-Gomez et al., 2017).

The anatomical processes associated with the formation of the fetal membranes have been well described (Benirschke et al., 2006; Hamilton and Boyd, 1960; Boyd and Hamilton, 1967). The first month of placental development proceeds in a uniform fashion, with the expansion and establishment of villi surrounding the entire developing embryo. These villi have the same complement of trophoblasts as more mature villi including diploid cytotrophoblast (CTB) and multinucleate syncytiotrophoblast (STB) [Knöfler et al., 2019]. The villi surrounding the embryo expand, branch, and are colonized by the fetal vasculature until 6-7 weeks of gestation, when degeneration begins in the future smooth chorion. In this region, villi continue to recede towards the basal plate. By the time the process is complete in the second trimester, villi are restricted to the discoid placenta that gives rise to the CTBs that invade the decidua (Hamilton and Boyd, 1960; Knöfler et al., 2019). As the developing fetus expands into the uterine cavity, the fetal membranes become juxtaposed to the decidual wall away from the discoid placenta, eventually fusing with these maternal cells at approximately 18 weeks of gestation. (Boyd and Hamilton, 1967).

The fetal membranes have a complex cellular makeup, which includes amniocytes, mesenchymal stromal cells, immune cells, and CTBs (Benirschke et al., 2006). The CTBs of the smooth chorion persist until term as an epithelial like structure. Non-functional “ghost villi” can occasionally be found in the smooth chorion, but lack STBs and fetal vasculature, and thus cannot function in a manner comparable to the chorionic villi (Benirschke et al., 2006). Furthermore, in contrast to the villous chorion where CTBs invade and remodel the maternal arteries, the CTBs of the smooth chorion do not invade the adjacent decidua and the maternal blood vessels it contains (Genbacev et al., 2015). Thus, the function of these CTBs remains unclear.

Several pieces of evidence suggest that the smooth chorion is not simply a vestigial structure. First, an intact CTB layer, which contains proliferating cells persists through the final 20 weeks of gestation (Yeh et al., 1989; Benirschke et al., 2006, 1979; Garrido-Gomez et al., 2017). Second, the histological heterogeneity among smooth chorion CTBs suggests functional distinctions. Yeh et al. (1989) characterize two distinct populations of vacuolated and eosinophilic CTBs. Vacuolated CTBs were positive for placental lactogen and placental alkaline phosphatase, while the eosinophilic subpopulations was not. Both populations were rich in keratin and neither had the known characteristics of villous CTBs. Bou-Resli et al. (1981) also

note high levels of variation among CTBs in the smooth chorion and the existence of a vacuolated population. A more molecular characterization was carried out by Garrido-Gomez et al. (2017), which demonstrated heterogeneity of ITGA4 and HLA-G expression, markers previously associated with stemness and invasion, respectively (Genbacev et al., 2016, McMaster et al., 1995). This study also uncovered an expansion of the smooth chorion in cases of severe pre-eclampsia, along with a disease-specific gene expression pattern. In sum, these results suggest the smooth chorion CTBs are a heterogeneous and dynamic collection of cells with important functions in development and disease.

Single cell RNA-sequencing (scRNA-seq) has emerged as the standard for transcriptional characterization of complex organs. This methodology was previously applied to the placenta, but with a focus on the maternal-fetal interface, specifically the chorionic villi and basal plate (Liu et al., 2018; Suryawanshi et al. 2018; Vento-Tormo et al., 2018). Recently, scRNA-seq was used to profile the fetal membranes at term. However, in this study CTBs were not identified in the smooth chorion, possibly due to apoptosis and/or changes in the membrane at term (Pique-Regi et al., 2019; Yuan et al., 2006; Yuan et al., 2008; Yuan et al., 2009). To fill this information gap, we applied scRNA-seq to matching samples of cells isolated from the villous and smooth chorion regions of human samples from late in the second trimester. We used scRNA-seq to compare the composition and developmental trajectories of CTBs in the villous and smooth chorion. The data were validated and extended with functional studies. These results identified a novel smooth chorion-specific CTB population important for establishment of a protective barrier and the suppression of trophoblast invasion. In addition, these data represent a resource of CTB types, proportions, and gene expression at mid-gestation against which age related and pathogenic alterations can be measured.

Results

The transcriptional landscape of the villous and smooth chorion at mid-gestation.

To understand the cellular composition of the smooth chorion, we isolated and profiled cells from both the villous (VC) and the smooth chorion (SC) regions of four second trimester human placentas spanning gestational weeks 18 to 24 (GW18-24) using single cell RNA-sequencing (Figure 1a). We chose to analyze second trimester samples because the maturation of the smooth chorion is complete but the inflammation and apoptosis associated with membrane rupture and parturition is absent (Benirshcke et al., 2006; Yuan et al., 2006; Yuan et al., 2008; Yuan et al., 2009; Figure 1a). For the purpose of establishing internal and patient controls purposes we isolated SC and VC cells from each human placental sample. CTBs were enriched over stromal and immune cells by using our previously published method (Garrido-Gomez et al. 2017). The transcriptomes of the resulting cells were captured using the 10x Genomics scRNA-seq platform.

Each of the eight datasets (GW17.6, 18.2, 23.0, 24.0; VC and SC) were captured independently, then integrated computationally (Figure 1b; Stuart et al., 2019). We classified the cells of the integrated dataset into broad cell type clusters according to functional identities and annotated each by expression of canonical markers. CTBs were annotated as *KRT7*+, *HLA-G*$^{-}$; extravillous trophoblasts (EVTs) as *KRT7*+, *HLA-G*+; immune cells as *CD45*+, *VIM*-; stromal cells as *VIM*+,

136 *CD45*-; and the uterine epithelium by expression of *EPCAM*+, *MUC1*+ and *MUC16*+ (Figure 1c;
137 Lee et al., 2016; McMaster et al., 1995; Vento-Tormo et al., 2018). Cells expressing exclusive
138 markers of disparate cell types (co-expression of *KRT7, HLA-G, HLA-A, VIM, ACTA2*) were
139 labelled as doublets and excluded from further analysis. The complete dataset used for further
140 analysis contained 50,496 cells that passed quality control (between 500 and 6500 unique
141 genes, fewer than 15% mitochondrial reads, doublets removed) [Figure 1-S1a; McGinnis et al.,
142 2019]. Cells originating from each placental region (VC - 25,367 and SC – 25,129) and each
143 placental sample (7,181-17,705 cells per sample) were well represented (Figure 1b; Figure S1b
144 and c). The number of cells in each broad cell type cluster demonstrated enrichment for CTB,
145 which represent more than 60% of the cells in the integrated dataset (Figure 1-S1d).
146

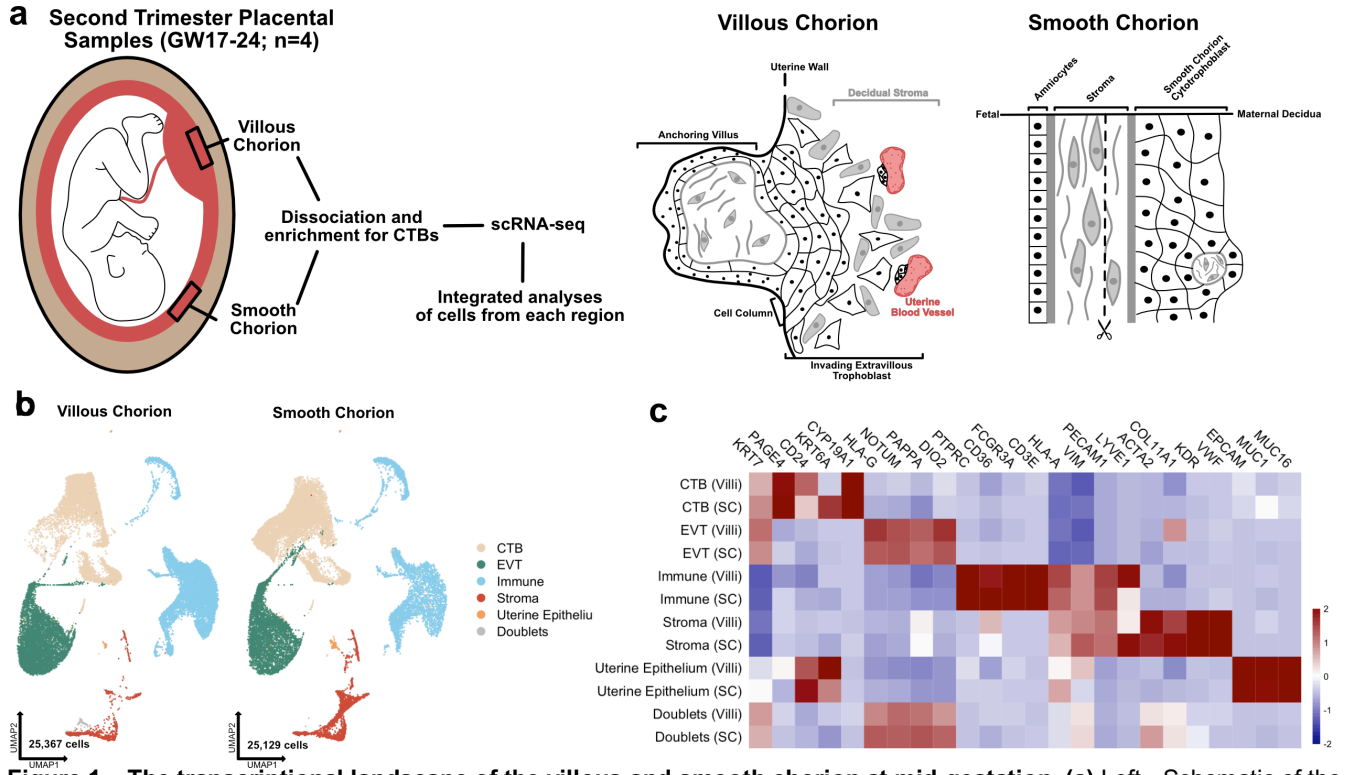

Figure 1 – The transcriptional landscape of the villous and smooth chorion at mid-gestation. (a) Left - Schematic of the placenta at mid-gestation, highlighting the regions sampled, together with the methods used for cell isolation and characterization. Right – schematic of the cell types and their organization in each region. **(b)** UMAP projections of integrated samples, shown by region of origin (Left – VC, Right – SC), and colored according to broad cell type clusters. **(c)** Heatmap of the transcript expression of select cell identity markers across broad cell type clusters and regions. Values are scaled expression across the clusters of each region independently.

147 While the enrichment protocol was designed to enrich for CTBs cells, several immune and
148 stromal subtypes were recovered, providing insight into the composition of these cells from each
149 region. The immune and stromal cells were subset and re-clustered, allowing the annotation of
150 subtypes within each group (Figure 1-S2a and b; Figure 1-S3a and b). The majority, if not all,
151 immune cells were of maternal origin (Figure 1-S2c). Almost two-fold more immune cells were
152 recovered from the VC than the SC, although it cannot be ruled out that this change in proportion
153 is not an artifact of dissection or enrichment protocol (Figure 1-S2d). Comparing the immune cell
154 types identified in each region revealed a higher proportion of macrophages in the VC as
155 compared to the SC, which contained a greater proportion of NK/T cells (Figure 1-S2e). These
156 differences may reflect the fact that SC samples contain a higher proportion of decidua and its

157 resident immune cells than their VC counterparts. Additionally, this result may suggest
158 differences in the maternal immune cells that interact with the two compartments.
159
160 While few stromal cells were isolated in the preparations, sub-clustering still revealed a
161 differential composition of fetal stromal cells between the VC and SC (Figure 1-S3a and b). The
162 majority of stromal cells recovered originated from the SC (2,941 compared to 942 from VC).
163 These cells included lymphatic endothelium (Pique-Regi et al., 2019) and two largely SC-specific
164 mesenchymal cell populations of fetal origin, Mesenchyme 1 and Mesenchyme 3 (Figure 1-S3c-
165 e). These two clusters are marked by elevated expression of *EGFL6*, *DLK1*, and uniquely by
166 expression of *COL11A1*, which is observed only in the SC (Figure 1-S3 b and f). Interestingly,
167 several canonical CTB support factors including HGF, WNT2, and RSPO3, were expressed in
168 fetal stromal populations in both placental regions, suggesting shared requirements for WNT
169 and MET signaling (Figure 1-S3g). Taken together these data demonstrate the identification of
170 broad classes of CTBs, immune, and support cells from both the VC and SC regions of the
171 human placenta.
172
173 **Identification of a smooth chorion-specific cytotrophoblast population.**
174 CTBs are the fetal cells that perform the specialized functions of the VC, and are required for
175 normal fetal growth and development (Maltepe and Fisher, 2015; Turco and Moffett, 2019;
176 Knöfler et al., 2019). To better understand the composition of CTBs in the SC versus the VC, we
177 sub-clustered this population (*KRT7*+, *VIM*-, *CD45*-, *MUC1*-). The CTB subset is comprised of
178 29,668 cells with similar representation and cell quality control metrics across all eight samples
179 (Figure 2-S1a, b, and c). This analysis identified 13 clusters including several CTB, EVT, and
180 STB subtypes (Figure 2a).
181
182 Broad classes of trophoblast were annotated by established markers (STBs - *CGA*, *CYP19A1*,
183 *CSH1*, *CSH2*; EVTs - *HLA-G, DIO2*; CTBs - *PAGE4*, *PEG10,* and no expression of EVT and
184 STB markers) [Figure 2b and Figure 2-S2a; McMaster et al., 1995; Lee et al. 2016, Suryawanshi
185 et al. 2018, Liu et al. 2018]. Two cell clusters showed high expression of canonical phasic
186 transcripts, including *MKI67*, with the S-phase cluster denoted by expression of *PCNA* and the
187 G2/M-phase cluster by expression of *TOP2A* (Figure 2-S2b; Tirosh et al. 2015). Both populations
188 share gene expression with all clusters of CTBs, and therefore, were identified as actively cycling
189 (Figure 2-S2a). No STB or EVT markers were identified in the cycling clusters as was expected
190 due to the requirement for cell cycle exit upon terminal differentiation to these lineages (Lu et al.
191 2017, Genbacev et al., 1997).
192
193 CTBs separated into four clusters, CTB 1-4. CTB 1 cells highly expressed *PAGE4*, *PEG10*, and
194 *CDH1* (Figure 2b, Figure 2-S2a, Figure 2-S3a), which have been shown to be canonical markers
195 of villous CTB (Lee et al. 2016, Suryawanshi et al. 2018). Overall, CTB 2-4 were more
196 transcriptionally similar to each other than to CTB 1, indicating a transcriptional program that
197 was distinct from canonical villous CTBs (Figure 2-S2a and c). CTB 2-4 existed along a gradient
198 of gene expression changes suggestive of various stages of a common differentiation pathway.
199 However, each population expressed distinct transcripts corresponding to important proposed
200 functions of the smooth chorion. CTB 2 cells highly expressed *CLU*, *CFD*, and *IFIT3*, suggesting

201 roles in responding to bacterial or viral infection through the innate arm of the immune system
202 (Thurman and Hollers., 2006; Liu et al., 2011). CTB 3 cells upregulated *EGLN3* and *SLC2A3*,
203 indicating a HIF-mediated response to hypoxia and a switch toward glucose metabolism, likely
204 as an adaptation to the decreased oxygen levels in the largely avascular smooth chorion region
205 (del Peso et al. 2003, Maxwell et al., 1997). Finally, CTB 4 specifically expressed several
206 cytokeratins — *KRT6A*, *KRT17*, and *KRT14*, found in many epithelial barrier tissues and
207 important for maintenance of integrity in response to mechanical stressors (Karantza, 2011;
208 Figure 2b, Figure 2-S2a). These results establish a previously underappreciated transcriptional
209 diversity of CTB subpopulations.
210
211 Quantification of cells showed a strong regional bias in the number and proportion contributing
212 to each CTB cluster (Figure 2c and d). In the VC samples, 53.8% of CTBs clustered in CTB 1
213 compared to 11.1% in the SC (Supplementary Table 1). In contrast, the SC had a much larger
214 proportion of the CTB 2-4 clusters. In this region, 71.3% of CTBs were nearly equally distributed
215 among CTB 2 (25.6%), CTB 3 (24.9%), and CTB 4 (20.8%). In the VC, only 24.1% of CTBs were
216 found in the same clusters, with the majority in CTB 2 (16.1%). The contribution to cycling
217 clusters was consistent across regions: 22.1% and 17.5% of CTBs in the VC and SC,
218 respectively. The relative proportions of CTB 1-4 in the VC and SC were consistent across
219 individual samples indicating that this difference was biological rather than driven by sample
220 variability or an artifact of sample integration (Figure 2-S1b-c).
221
222 Next, we immunolocalized the protein products of genes that distinguished the subpopulations.
223 At the mRNA level, *PAGE4* expression was highest in CTB 1 and decreased across CTB 2-4
224 (Figure 2b and e). In the VC, the CTB monolayer between the fetal mesenchymal villous core
225 and the overlying STB layer showed strong PAGE4 immunoreactivity, which diminished upon
226 differentiation to EVT (Figure 2f - left). PAGE4 mRNA and protein expression matched that of
227 known villous CTB marker CDH1 (Figure 2-S3a and b; Zhou et al., 1997). In the SC, the PAGE4
228 signal was strong in the epithelial layer directly adjacent to the fetal mesenchyme and then
229 decreased in cells distant from the basal layer, again matching CDH1 (Figure 2f - right, Figure
230 2-S3b - right). Both RNA expression and protein localization were consistent with CTB 1 cells
231 existing on both sides of the placenta and occupying a similar niche.
232
233 Staining for KRT6, a marker highly enriched in CTB 4 cells (Figure 2g) showed a strikingly
234 different result. Cells occupying the upper layers of SC epithelium showed a strong KRT6 signal,
235 a pattern opposite to CDH1 (Figure 2h and i - right). KRT6 was absent from either the floating
236 or anchoring villi of the VC (Figure 2h and i - left). Rare decidual resident KRT6 positive CTBs
237 were also identified in the VC region. (Figure 2-S3c, Figure 6-S1 - top). KRT6 isoforms, KRT6B
238 and KRT6C, were not expressed, confirming KRT6A transcript and protein as highly specific
239 markers of a CTB population found only in the smooth chorion (Figure 2-S3d). These data
240 describe a novel subpopulation of CTBs unique to the SC, which going forward we term CTB 4
241 or SC-CTBs for smooth chorion-specific CTBs.
242

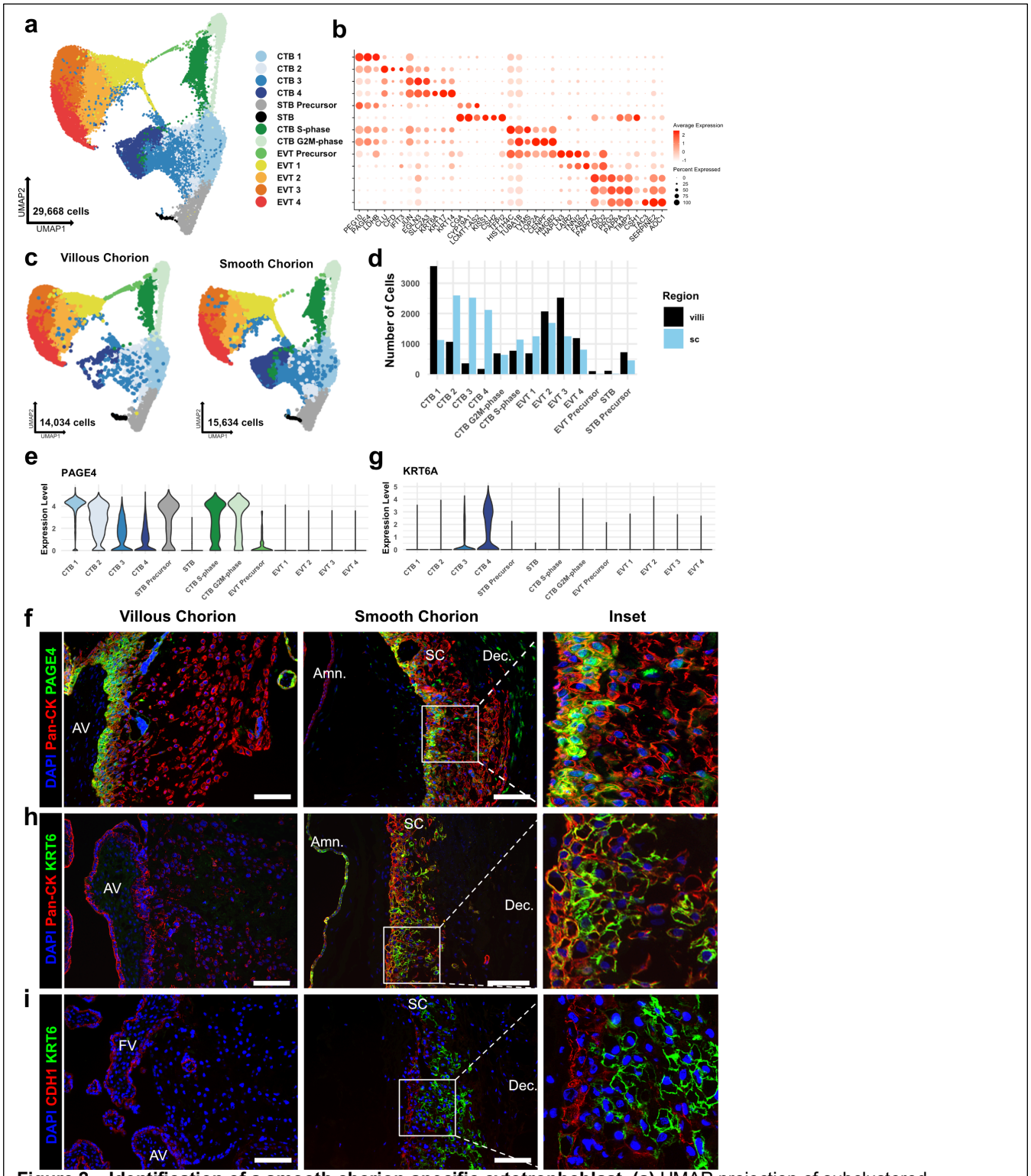

Figure 2 – Identification of a smooth chorion-specific cytotrophoblast. (a) UMAP projection of subclustered trophoblasts (n=29,668). Colors correspond to the clusters at the right. **(b)** Dot plot showing average expression and percent of cells in each cluster as identified by the marker genes listed on the x-axis. The clusters are listed on the y-axis. **(c)** UMAP projection of subclustered trophoblasts from the VC (Left) or the SC (Right). Clusters and colors are the same as in panel a. **(d)** Quantification of the number of cells in each trophoblast cluster from each region. Cells from the VC are shown in black. Cells from the SC are shown in blue. **(e)** Violin plot of *PAGE4* transcript expression across all trophoblast clusters. **(f)** Immunofluorescence co-localization of PAGE4 with pan-cytokeratin (marker of all trophoblast) in the VC (Left) or SC (Right). **(g)** Violin plot of *KRT6A* transcript expression across all trophoblast clusters. **(h)** Immunofluorescence co-localization of KRT6 with pan-cytokeratin (marker of all trophoblast) in the VC (Left) or SC (Right). **(i)** Immunofluorescence co-localization of CDH1 and KRT6 in the VC (Left) or SC (Middle). High magnification inset is denoted by the white box (Right). For all images nuclei were visualized by DAPI stain; Scale bar = 100μm. Abbreviations: AV = Anchoring Villi; FV = Floating Villi; SC = Smooth Chorion epithelium; Amn. = Amnion; Dec. = Decidua.

A common CTB progenitor gives rise to STBs in the VC and SC-CTBs in the SC.

Next, we investigated the developmental origin of the SC-CTBs. We performed RNA velocity analysis to predict the relationships between cells based on the proportion of exonic and intronic reads. These predictions are shown as vectors representing both the magnitude (predicted rate) and the direction of differentiation (Bergen et al. 2020). We first asked whether RNA velocity could recapitulate the well-established differentiation trajectories of trophoblasts in the VC (Knöfler et al., 2019; Turco and Moffett, 2019; Vento-Tormo et al. 2018). In accordance with previous results, RNA velocity projections identified CTB 1 as the root for three differentiation trajectories: self-renewal, differentiation to STBs, and differentiation to EVTs (Figure 3a). Cells at the boundary of the CTB 1 cluster showed differentiation vectors of high magnitude toward STB Precursors and upregulated canonical drivers of STB differentiation and fusion (*ERVW-1* and *ERVFRD-1*). These cells also expressed transcription factors (*GCM1* and *HOPX*) and hormones (*CSH1*) necessary for STB function (Figure 3-S1a; Baczyk et al., 2009; Mi et al., 2000; Blaise et al., 2003; Yabe et al., 2016).

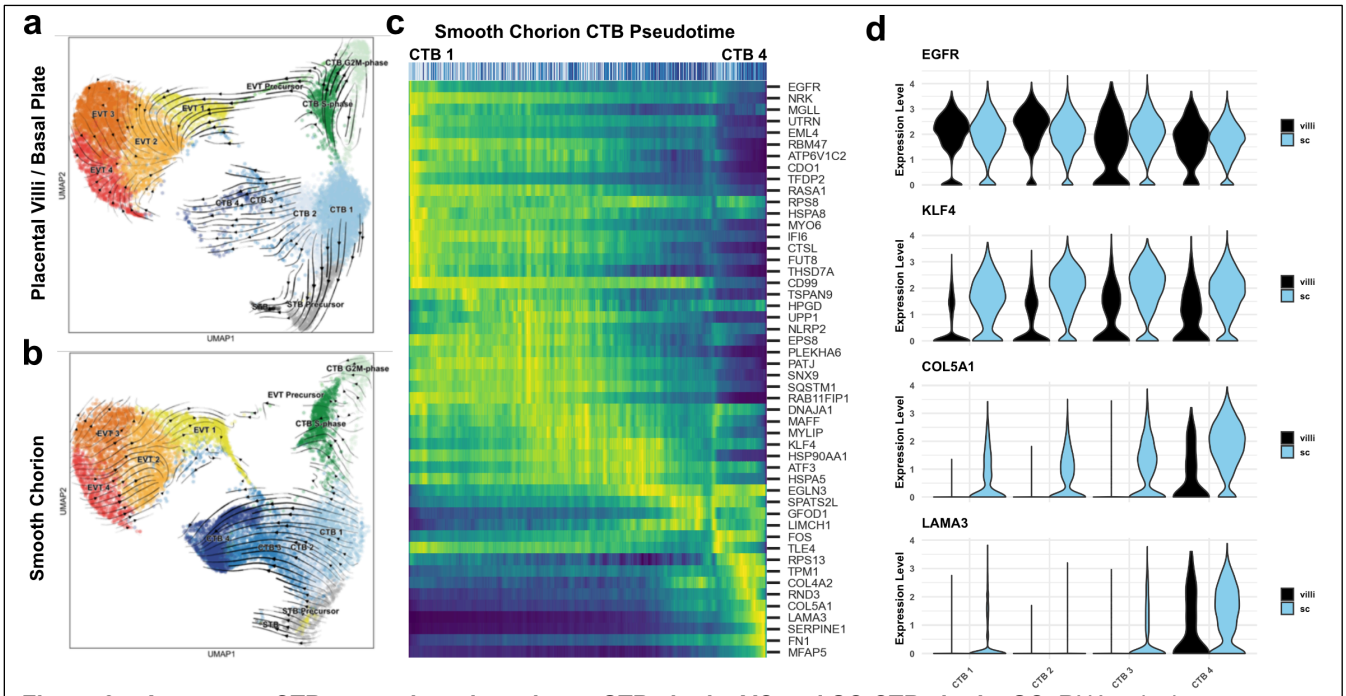

Figure 3 – A common CTB progenitor gives rise to STBs in the VC and SC-CTBs in the SC. RNA velocity vector projections overlaid on to UMAP projections for trophoblast cells isolated from the **(a)** VC and **(b)** SC. Arrows denote direction and magnitude is represented by line thickness. **(c)** Pseudotime reconstruction of SC derived CTB 1-4 clusters from the scVelo dynamical model of latent time. Each column represents one cell. Cells at the left are clustered in CTB 1 and progress through CTB 2, 3, and 4 along the x-axis. Select genes that were the major drivers of the pseudotime alignment are shown on the y-axis. Expression ranged from dark blue (lowest) to yellow (highest). **(d)** Violin plots of select factors from (c) demonstrated shared or region-specific expression for genes associated with the CTB 4 differentiation trajectory.

In the SC, CTB 1 cells once again were identified as the root for differentiation. However, CTB 1 cells showed strong directionality and magnitude toward CTB 2-4 (Figure 3b). All cells in CTB 1-4 clusters displayed uniform directionality indicating a robust differentiation trajectory ending at CTB 4. High levels of transcriptional similarity between CTB 2-4 compared to CTB 1 suggested CTB 2 and 3 are intermediate states between CTB 1 and CTB 4 (Figure 2-S2c). Mitotic KRT6+ cells were identified, suggesting that differentiation to SC-CTB does not require cell cycle exit (Figure 3-S1b). In contrast to the VC, we observed no velocity vectors with

directionality toward the STB lineage from the CTB clusters in the SC samples. Further, the smaller number of STB precursors (460 cells) and STBs (14 cells) exhibited reduced expression of STB canonical markers such as ERVFRD-1 and GCM1, and notably, a near absence of ERVW-1 (Figure 3-S1a). These cells may be associated with ghost villi (Benirschke et al., 2006). In sum, these data show differential developmental trajectories for the CTB 1 cells in the SC and VC, with the former largely giving rise to SC-CTBs and the latter to STBs.

To identify the genes that were correlated with progression from CTB 1-4 in the SC, we used the velocity vector predictions to construct a pseudotemporal model of differentiation. All the cells in these clusters were plotted in one dimension from the least to the most differentiated according the pseudotime model (Figure 3c). Genes that were highly expressed at the start of the pseudotemporal differentiation included pan-trophoblast factors such as *EGFR*, which was expressed throughout all four CTB populations in both the VC and SC. Progression along the pseudotime trajectory identified regulators of cell fate and function, including the transcription factor *KLF4* and extracellular matrix (ECM) components *COL5A1* and *LAMA3* (Figure 3c-d); all demonstrated SC-specific expression. Elevated expression of ECM transcripts (*COL4A2*, *FN1*) and transcription factors responsive to cell contact and mechanical stress *(HES1*, *YAP1)* were coordinately upregulated, potentially highlighting the effects of the extracellular environment on fate specification (Figure 3-S1c). These data demonstrated that SC-CTBs originate from CTB 1 progenitors common to both the VC and SC. In the SC, instead of upregulating syncytialization factors such as *GCM1* and *ERVFRD-1*, CTB 1 progenitors upregulate transcription factors such as *KLF4*, *YAP1*, and *HES1*, which drive an epithelial cell fate in other contexts (Segre et al., 1999, Harvey et al., 2013; Rock et al., 2011).

SC-CTBs express a distinct epidermal transcriptional program.

Next, we sought a better understanding of the physiological functions of the SC trophoblast clusters. We performed gene ontology analysis as a summary of functional processes (Figure 4a, Figure 4-S1; Yu et al., 2012). We focused on the progenitor CTB 1 and terminally differentiated SC-CTBs as they showed enrichment for strikingly different functional categories. In CTB 1, we identified enrichment for WNT signaling, epithelial morphogenesis, and membrane transport, categories commonly associated with progenitors (Figure 4a, Figure 4-S1). We validated the activity of WNT signaling and the location of these cells by immunolocalization of non-phosphorylated CTNNB1 (intact form of the protein). β-Catenin was localized to the most basal epithelial layer nearest to the stroma in both the VC and SC regions (Figure 4b), matching expression of the CTB 1 marker CDH1 (Figure 4-S2a). WNT signaling has an important role in the maintenance of villous CTBs *in vivo* and in the derivation and culture of self-renewing human trophoblast stem cells (Knöfler et al., 2019; Haider et al., 2018; Okae et al., 2018). We investigated proliferation of CTNNB1 expressing cells in both regions using KI67 as a mitotic marker. This revealed a similar percentage of KI67+ CTB 1 cells, suggesting similar proliferative capacity across regions (Figure 4b and c). We next analyzed regional differences within CTB 1. Gene ontology identified an enrichment for oxidative phosphorylation and epithelial signaling cues in VC CTB 1 cells (Figure 4-S2b). This is in direct contrast to SC CTB 1 cells that displayed elevated levels of hypoxia response genes (Figure 4-S2b-c). KLF4 was identified in the RNA velocity analysis as gaining expression from CTB1-4, but also showed greater expression in

CTB1 in the SC compared to the VC (Figure 3d). In accordance with the mRNA expression data, KLF4 protein often co-localized to CTB1 in the SC, but was only observed in rare cells in the VC (Figure 4d). These data further support a similar location and function for CTB 1 in the SC and VC, with transcriptional and metabolic differences that presage distinct developmental trajectories.

CTB 4 ontological analysis strongly supported important roles for these cells in the formation of a protective barrier. The greatest enrichment was for cell junction and cell substrate adhesion genes that included numerous integrin and laminin subunits as well as junctional proteins *PATJ*, *DSP*, and *JUP*. An enrichment for both skin and epidermal development correlated with upregulation of the ECM and junctional transcripts. These categories included many cytokeratins (*KRT6A, 7, 8, 14, 17, 18,* and *19*) and transcription factors (*KLF4*, *YAP1)* required for epidermal identity and maintenance (Segre et al., 1999; Schlegelmilch et al., 2011). The organization of the SC is reminiscent of stratified epidermal cells of the skin, with progenitors adherent to the basal lamina and more differentiated cells progeny forming the upper layers. In many tissues, the specific domains of cytokeratin expression correspond to stratified cell layers with different functions. We asked if this was also the case in the SC epithelium. Cytokeratins 7, 8, and 18

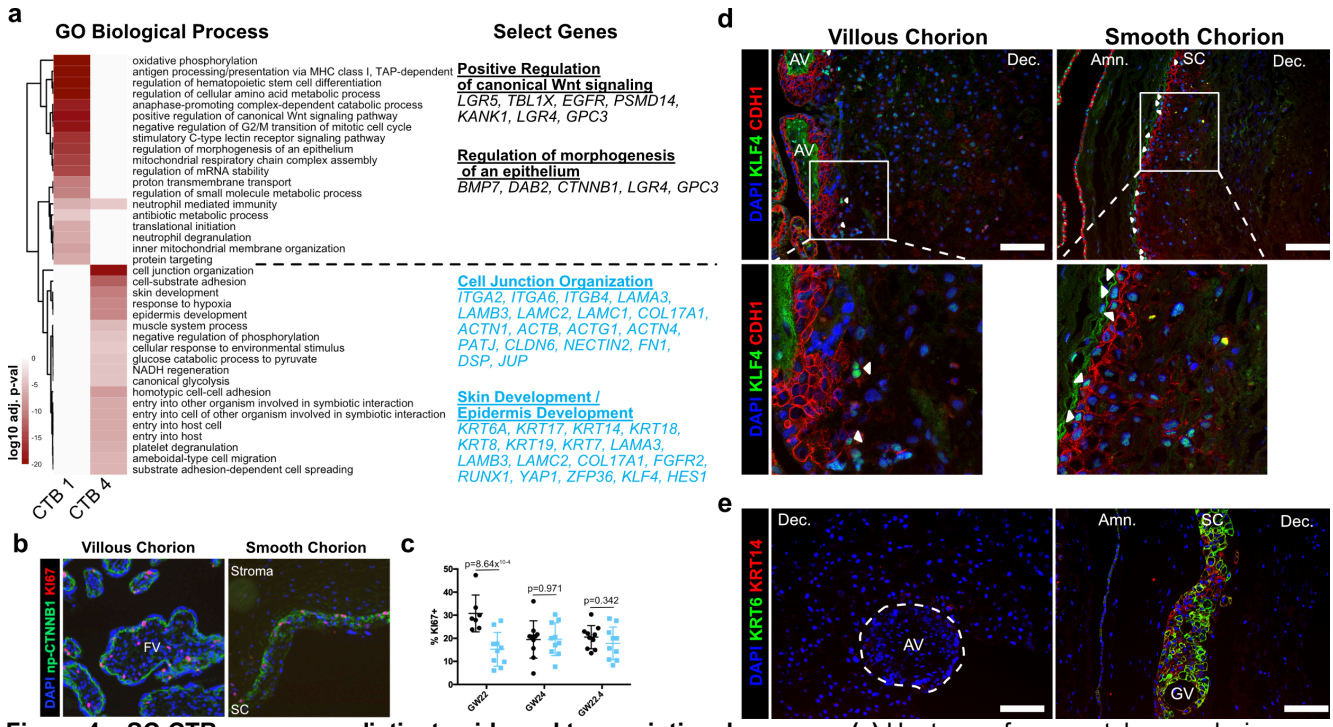

Figure 4 – SC-CTBs express a distinct epidermal transcriptional program. (a) Heatmap of gene ontology analysis adjusted p-values. Dark red corresponds to the lowest p-values and white represents p-values greater than 0.0005. Ontology categories are organized by hierarchical clustering along the y-axis. Marker genes for each cluster were used as inputs for the analysis. A subset of genes in selected categories are listed at the right. Categories and genes enriched in CTB 1 or CTB 4 are in black or blue, respectively. **(b)** Representative immunofluorescence co-localization of non-phosphorylated CTNNB1 and KI67 in the VC (Left) and SC (Right). **(c)** Quantification of the percent of np-CTNNB1 cells with KI67 expression in each region in three placental samples. Each dot represents the percentage in one field of view (at least 7 per region per sample) as an estimate of mitotic cells per population. Percentages for the VC region are shown in black and the SC region in blue. **(d)** Immunofluorescence co-localization of CDH1 and KLF4 protein in the VC (Left) or SC (Right). Arrowheads denote CDH1+/KLF4+ cells. **(e)** Immunofluorescence co-localization of KRT14 and KRT6 protein in the VC (Left) or SC (Right). The outline of the Anchoring Villi (AV) is denoted by the white dashed line. For all images nuclei were visualized by DAPI stain; Scale bar = 100μm. Abbreviations: AV = Anchoring Villi; FV = Floating Villi; SC = Smooth Chorion epithelium; Amn. = Amnion; Dec. = Decidua; GV = Ghost Villi.

were expressed in all trophoblast regardless of region (Figure 4-S3a), but cytokeratin 6A, 14, and 17 displayed smooth chorion-specific expression that increased with differentiation towards CTB 4 (Figure 4-S3b). Immunofluorescence localization confirmed expression of KRT14 as specific to the CTBs in the SC and inclusive of all KRT6 expressing cells (Figure 4e). These data support a model of accumulated cytokeratin expression that begins with CTB 1 (*KRT7, KRT8, KRT18*), increases in CTB 2-3 (*KRT14, KRT17*), and culminates in CTB 4 (*KRT6A*). Together these data are consistent with a central role for the CTBs of the SC in establishing a protective epithelial barrier for the rapidly growing fetus.

Beyond forming a physical barrier, important placental functions include protection from bacterial and viral infections. We identified an enrichment for genes involved in antiviral response in SC-CTBs, and in SC cells more broadly. For example, IFITM3, a restriction factor preventing entry of viruses into cells, is highly expressed in CTBs from the SC compared to the VC (Figure 4-S4; Bailey et al., 2014; Spence et al., 2019). IFITM proteins have also been reported to inhibit syncytialization (Buchrieser et al. 2019), suggesting IFITM3 may also function to block differentiation of CTBs into STBs in the SC. Taken together, these data establish SC-CTBs as the building blocks and critical regulators of the SC barrier, responsible for both protection against physical forces and pathogen infection.

EVTs of the VC and SC regions are behaviorally distinct but transcriptionally similar.

EVTs are the invasive trophoblasts of the placenta (Knöfler et al., 2019; Turco and Moffett, 2019; Red-Horse et al., 2004). While the EVTs of the VC migrate away from the villi, invade the decidua, and replace the endothelial lining of the uterine arteries, the EVTs of the SC adhere to the decidua and do not home to the maternal vasculature (Genbacev et al., 2015). To understand the basis for these differences, we compared EVT subpopulations isolated from the VC and SC. Expression of the canonical marker of EVTs, *HLA-G*, was similarly abundant among the cells isolated from both placental regions (Figure 5a and b). A greater number (VC - 6572; SC - 5021) and larger proportion (VC – 46.83%; SC – 32.12%) of CTBs from the VC expressed HLA-G as compared to the analogous population from the SC (Figure 5c). Consistent with the transcript expression data, immunolocalization of HLA-G showed strong staining of cells in both the VC and SC. However, VC derived HLA-G positive cells were found deep in the maternal decidua. In contrast, HLA-G positive cells in the SC remained in the epithelial layer (Figure 5b).

EVTs were further divided into clusters 1-4. No clusters were specific to the VC or SC, except for the small number of putative EVT Precursors (VC – 99 cells; SC – 8 cells) [Figure 5d, Figure 3a]. Previous work has classified EVTs on the villous side of the placenta as columnar, interstitial, or endovascular based on behavior and location in the decidua (Tilburgs et al., 2015; Knöfler et al., 2019). The columnar subpopulation is believed to represent newly differentiated EVTs, which lie at the base of the columns that connect the anchoring villi to the uterine wall. Interstitial EVTs migrate through the decidua homing to maternal arteries, which they invade. Within the arterial wall, this subpopulation further differentiates to endovascular EVTs and replaces the maternal arterial endothelium (Harris et al. 2009, Red-Horse et al. 2004). We expected to capture both columnar and interstitial EVT populations, but few endovascular EVTs as the cellular preparations were largely devoid of arteries. We investigated the four clusters of EVT identified

371 in our analysis in the context of the VC and the SC. Both placental regions contained cells from
372 all clusters, although distinct regional biases were evident (Supplementary Table 1). The SC
373 region contained almost twice as many EVT 1 cells as the VC (VC – 684; SC – 1256), whereas
374 the VC contained almost twice as many EVT 2-4 as the SC (VC – 5789; SC – 3757). We next
375 asked which of the EVT clusters corresponded to known EVT classifications, indicating
376 maturation state or invasive capacity. Gene ontology analysis showed an enrichment for
377 placental development and antigen presentation categories in EVT 1 (Figure 5-S1a).
378 Representative marker genes for these categories in EVT 1 included several lineage-specific
379 transcription factors including *GCM1*, *PPARG*, and *CEBPB* (Figure 5-S1b; Knöfler et al., 2019,
380 Ferreira et al., 2016). In contrast, EVT 2-4 showed enrichment for extracellular structure and
381 matrix organization, glycosylation, and peptidase activity. EVT clusters 3-4 specifically showed
382 increased expression for transcripts of proteases such as *HTRA1*, *MMP2*, and *MMP11* (Figure
383 5-S1c). Based on the GO and specific gene enrichments, EVT 1 appeared most similar to
384 columnar EVTs, while EVT 2-4 were consistent with interstitial EVTs that gain invasive capacity.
385 The relative enrichment for EVT 1 in the SC (VC – 10.57% of EVT; SC – 25.05% of EVT)
386 suggested an expansion in columnar-like EVTs at the expense of interstitial EVT. Conversely,
387 the relative enrichment for EVT 2-4 in the VC region suggested an expansion of the invasive
388 subpopulation (Figure 5d).
389
390 As almost 75% of EVTs from the SC region were in EVT clusters 2-4, we next asked if there
391 were differences in gene expression between interstitial EVTs isolated from each region. This
392 analysis identified relatively few differentially expressed genes, with the vast majority identified
393 having a log fold change less than 1 (Figure 5-S2a). The small number of differentially expressed
394 genes with a fold change greater than 1 was typically identified across multiple EVT clusters,
395 suggesting an overriding transcriptional program that might supersede subcluster designations.
396 To identify genes associated with this program, we combined all EVT subclusters into one cluster
397 for analysis (Figure 5e). Differential expression analysis revealed the hormone CSH1 and
398 several proteases including HTRA1, HTRA4, and PAPPA to be expressed at significantly higher
399 levels in the more invasive VC EVTs. However, of the most differentially expressed transcripts
400 only CSH1, ITM2C, and DNASE1L3 were exclusive to the VC (Figure 5-S2b).
401 Immunolocalization of CSH1 confirmed this result (Figure 5f). CSH1, also known as human
402 prolactin, is a secreted hormone that signals through the receptor PRLR found on maternal cells.
403 As such, the primary effect of CSH1 is likely non-cell autonomous, raising the possibility that the
404 largest differences in EVTs between regions may not be in inherent invasive capacity, but rather
405 their ability to communicate with the neighboring cells.
406
407 We next asked whether the gene expression differences between the VC and SC were smaller
408 for EVT clusters than for all other trophoblast clusters. Calculating the Pearson Correlation
409 coefficient across each cluster, EVT 3, EVT 4, and CTB 1 (which we have established as
410 common to both regions) were most similar and the only clusters with a coefficient greater than
411 0.75 (Figure 5-S2c). Since this analysis does not account for cluster heterogeneity or size, we
412 quantified the number of differentially expressed genes between 100 randomly selected cells
413 from each placental region within each cluster. Across 100 permutations, the number of
414 differentially expressed genes between regions was the lowest for all four EVT clusters (Figure

5g). Together, these results showed that the EVTs of the VC and SC are surprisingly similar even though they have distinct behaviors *in vivo*, suggesting a cell non-autonomous, rather than cell autonomous, regulation of invasion.

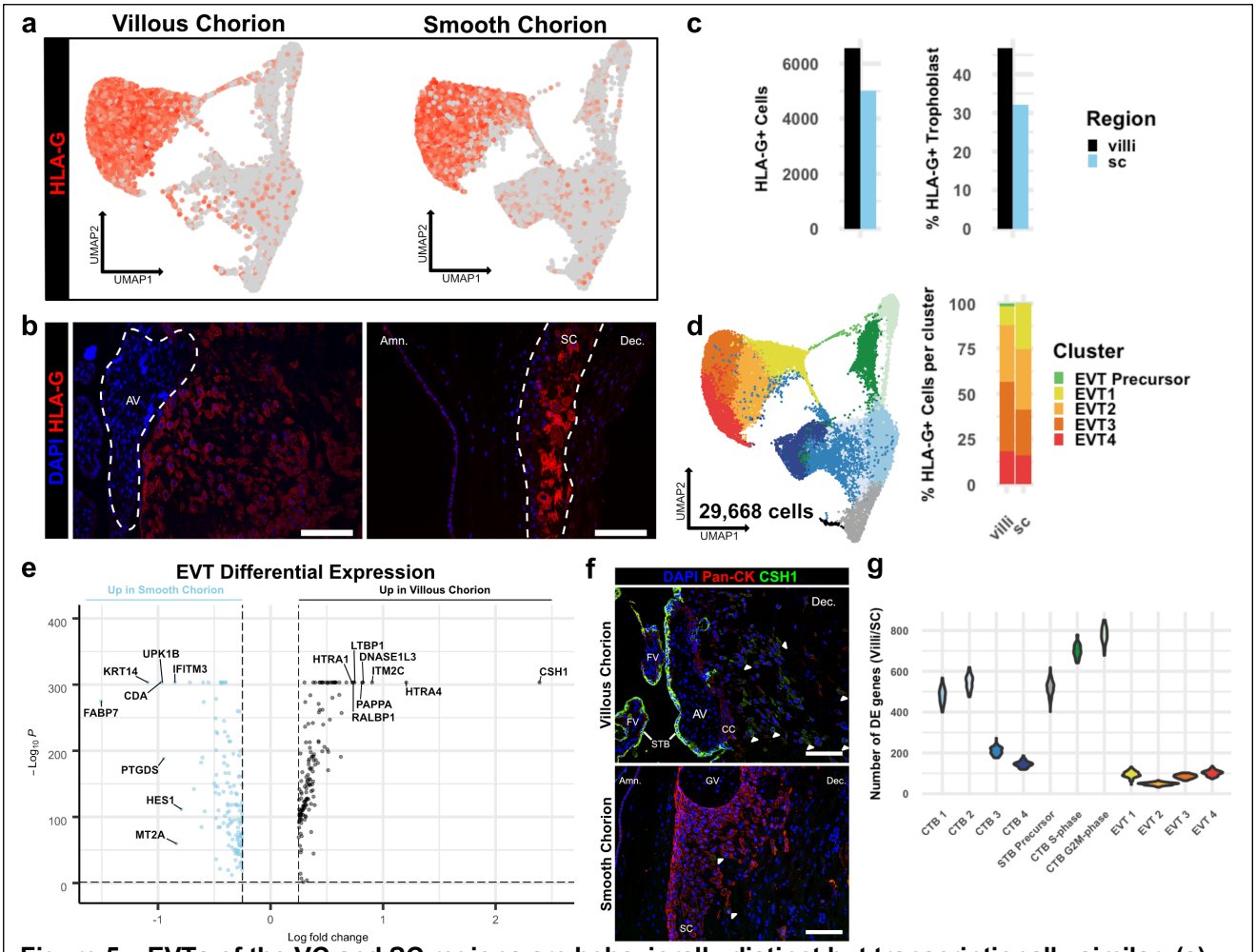

Figure 5 – EVTs of the VC and SC regions are behaviorally distinct but transcriptionally similar. (a) Expression of *HLA-G* transcript per cell projected in UMAP space for the VC (Left) and SC (Right). Expression ranged from low in light gray to high in dark red. **(b)** Immunofluorescence localization of HLA-G in the VC (Left) and SC (Right). The Anchoring Villi (AV) are outlined in white (Left). The boundaries of the smooth chorion epithelium are denoted by the white lines (Right) **(c)** Quantification of the number of *HLA-G* expressing EVT (Left) and the percent of total trophoblast that express *HLA-G* (Right) for each placental region. **(d)** UMAP projection of all trophoblast cells including the EVT clusters (Left). The percent of EVT cells in each cluster from each region (Right). **(e)** Volcano plot of the differentially expressed genes between regions for all EVTs. All genes with a log fold change greater than an absolute value of 0.25 and a p-value of less than 0.05 were plotted. Those with greater expression in VC EVT are shown in black. Those with greater expression in SC EVT are shown in blue. **(f)** Immunofluorescence localization of CSH1 in the VC Top) and SC (Bottom). Arrowheads denote CSH1 expressing cells **(g)** Violin plots of the number of differentially expressed genes between 100 cells from each placental region within each cluster (100 permutations). Clusters with less than 100 cells per region were omitted due to the small sample size. For all images nuclei were visualized by DAPI stain; Scale bar = 100μm. Abbreviations: AV = Anchoring Villi; FV = Floating Villi; SC = Smooth Chorion epithelium; Amn. = Amnion; Dec. = Decidua; STB = Syncytiotrophoblast; CC = Cell Column.

CTBs of the SC inhibit EVT invasion.

Given the transcriptional similarity between EVT clusters originating from the VC and SC, we wondered if a non-cell autonomous program could explain their distinct migratory properties. Immunofluorescence co-localization of CTB 1, SC-CTBs, and EVTs showed striking differences in the relative positioning of the EVTs and CTBs in the two placental regions (Figure 6a and b).

On the VC side, which lacks SC-CTBs cells, HLA-G+ EVTs were distant from the np-CTNNB1+ CTB 1 cell population as expected (Genbacev et al., 2015). By the second trimester they had migrated away from the cell column of the anchoring villi into the uterine stroma (Figure 6a). In contrast, HLA-G+ EVTs in the SC were adjacent to and in physical contact with KRT6+ SC-CTBs (Figure 6b). The interactions between SC-CTBs and EVTs were numerous and widespread throughout the SC epithelium. Contacts between CTB 1 and EVTs in the SC were not observed and the VC contain only rare and irregular KRT6+ cells (Figure 6-S1). This close association suggested possible paracrine signaling events between SC-CTBs and EVTs, which might impact each cell type.

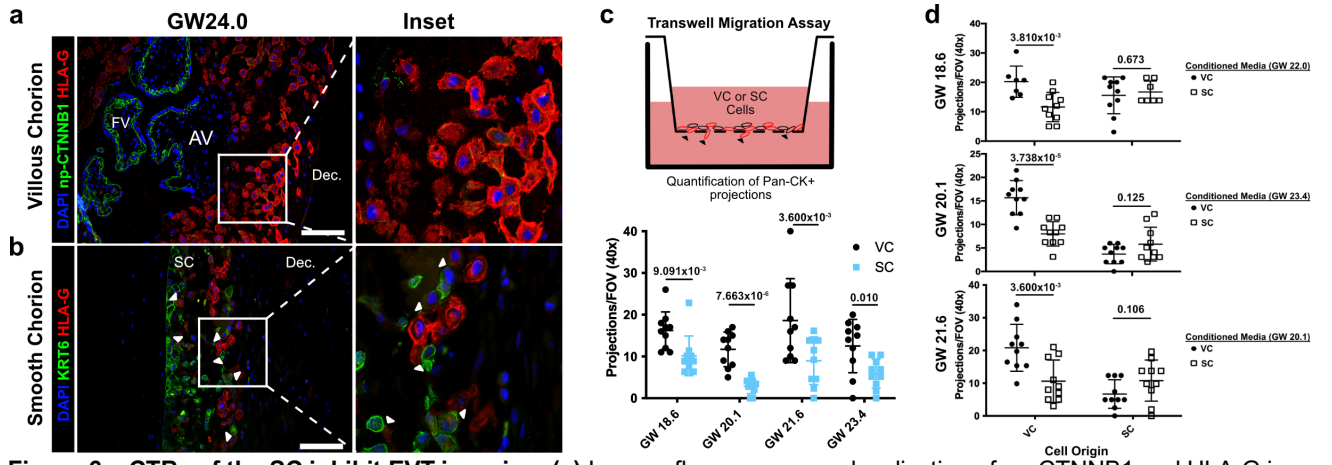

Figure 6 – CTBs of the SC inhibit EVT invasion. (a) Immunofluorescence co-localization of np-CTNNB1 and HLA-G in the VC. **(b)** Immunofluorescence co-localization of KRT6 and HLA-G in the SC. Arrowheads denote CTB and EVT interactions. **(c)** Schematic of the transwell invasion assay (top). Cells from either placental region were plated in the upper chamber of the transwell. After 39 hours of culture, the transwell membrane was fixed and stained with a Pan-cytokeratin antibody. The projections through the membrane are denoted by black arrowheads and quantified below. Results from the VC derived cells are shown in black, and the results from the SC derived cells are shown in blue. **(d)** Results from three biological replicates from each placental region cultured with conditioned medium from either VC or SC cells. The gestational ages of the plated cells is shown adjacent to the y-axis. The gestational ages of the cells from which conditioned medium was collected are noted in the legends at the right. The results for cells cultured with VC cell conditioned medium are denoted by black dots, and the results for those cultured in SC cell conditioned medium are denoted by open squares. P-values were determined by t-test and are listed above each comparison. For all images nuclei were visualized by DAPI staining ; Scale bar = 100μm. Abbreviations: AV = Anchoring Villi; FV = Floating Villi; SC = Smooth Chorion epithelium; Dec. = Decidua.

To test this theory, we attempted to recapitulate the differential invasive properties of VC and SC EVTs in a transwell migration assay. Briefly, these cells were enriched using the same protocol as described for the scRNA-seq experiments. The cells were plated on Matrigel coated transwell filters and cultured for 39 hours. Trophoblast projections that reached the underside of the filter, a proxy for invasion, were visualized by immunostaining with a pan-cytokeratin antibody (Figure 6c, Figure 6-S2). Consistent with the differences observed *in vivo*, there was greater invasion of VC as compared to SC trophoblast (Figure 6c). Next, we asked whether EVTs from the SC region secreted soluble factors that inhibited invasion. The invasion assays were repeated with VC cells cultured with conditioned medium from SC cells and vice versa. While VC conditioned medium had no impact on either VC or SC cells, SC conditioned medium significantly reduced migration of VC cells (Figure 6d). Neither conditioned medium impacted the density of VC or SC cells (Figure 6-S3). Therefore, a secreted factor from SC cells inhibited the migration of VC EVTs. Given that SC-CTBs were unique to the SC side, it is highly likely that they produced secreted factors that inhibit the invasion of EVTs to which they are juxtaposed.

449 **Discussion**
450
451 This study profiled the developing 2nd trimester placenta, providing a high-resolution molecular
452 description of the trophoblast in the smooth chorion and placing them in context of the
453 trophoblast from the VC of the same placenta. In doing so, we addressed long standing
454 observations concerning apparent similarities and differences between VC and SC trophoblast,
455 deconstruct the trophoblast populations in the SC, and ascribe functions to the cells of this
456 understudied region. Our study characterized a novel trophoblast population distinct from both
457 extant CTB in the VC and from EVT found in either placental region. These trophoblasts reside
458 only in stratified epithelium of the smooth chorion, express a specific cytokeratin (KRT6), and
459 comprise at least 25% of all trophoblast in the region. Lineage reconstruction by RNA velocity
460 suggested the progenitors for these smooth chorion-specific CTBs are a resident proliferative
461 progenitor trophoblast with a transcriptional profile that matches villous CTB. We identified
462 several potential regulators of the transition from a common villous CTB-like cell to SC-CTB,
463 including epidermal transcription factors such as KLF4 and YAP1. These molecules along with
464 region-specific signaling events drive an epidermal transcriptional program creating the building
465 blocks for a barrier against both physical and pathogen stressors. Finally, we identified CTB-
466 EVT interactions occurring only in the smooth chorion and provide evidence that paracrine
467 signaling between these populations restricts trophoblast invasion.
468
469 Since the smooth chorion is created by a degenerative process, consensus has been that these
470 cells are remnants of this process, making the smooth chorion a vestigial structure (Benirschke
471 et al., 2006). However, several previous observations suggested this might be an
472 oversimplification. First, these cells were noted to be proliferative, suggesting either cellular
473 expansion or turnover (Benirschke et al., 2006). We confirmed the presence of proliferative
474 trophoblasts in the smooth chorion. Each cycling CTB cluster expressed markers of CTB 1-4 in
475 both regions (Figure 2-S2a) and both CTB 1 (Figure 4b-c) and SC-CTBs (Figure 3-S1b) also
476 expressed KI67 protein. Proliferation of both the progenitor and differentiated cells suggested a
477 need for expansion coordinated with the growth of the developing fetus. Second, the importance
478 of the smooth chorion was suggested by the noted heterogeneity of the trophoblasts within this
479 region (Yeh et al., 1989; Bou-Resli et al., 1981; Garrido-Gomez et al., 2017; Benirschke et al.,
480 2006). In agreement, our scRNA-seq results showed the smooth chorion to be a complex tissue
481 with several trophoblast types. We identified, by differential transcription and function, at least
482 two distinct CTB cell types, columnar and interstitial EVT, and a small number of STB
483 Precursors. As discussed, all CTB and EVT populations either matched those found in the VC
484 or had new region-specific functions. The only evidence of degeneration was the STB Precursor
485 population within the smooth chorion, which lacked expression of both *ERVW-1* and *ERVFRD-*
486 *1*, the fusogens necessary to form STB (Mi et al., 2000; Blaise et al., 2003; Liu et al., 2018). In
487 sum, these studies suggested that the SC is a complex and functional tissue, not simply the
488 remnant of villous degeneration.
489
490 We focused on CTB 4, a novel population found exclusively in the SC, in the context of the
491 unique functions of this placental region. CTB 4 were enriched for epidermal, skin development,
492 and antiviral gene categories suggesting concerted roles in the creation of a barrier against

493 external forces and pathogens. Previous studies have noted that CTBs residing in the SC have
494 high levels of keratin expression and are associated with extensive ECM deposits rich in laminin,
495 collagen, and fibronectin (Yeh et al., 1989; Bou-Resli et al., 1981; Benirschke et al., 2006).
496 Among all smooth chorion CTB populations, but most notably in CTB 4, we identified the
497 upregulation of ECM components, including *LAMA3*, *COL5A1* and *FN1*. Expression of ECM
498 molecules in the SC is essential to protect against premature rupture of the fetal membranes,
499 but its deposition has previously been ascribed to stromal cells in the chorion (Parry and Strauss,
500 1998). This result also suggested that these trophoblasts create a specific ECM environment
501 distinct from other placental regions. This altered composition likely has wide-ranging effects on
502 trophoblast fate, gene expression, and behavior. It will be interesting to explore the impact of
503 advancing gestational age on the SC epithelium, especially with respect to the ECM.
504 Presumably, cellular and structural changes precede the normal process of membrane rupture
505 prior to delivery at term. Whether premature rupture of the membranes phenocopies these
506 events or is a unique process is an important open question.
507
508 Pathogen defense is another important function of the placenta. Infections of the chorion and
509 amnion (chorioamnionitis) often result in adverse outcomes for mother and fetus, primarily
510 preterm birth (Romero et al., 2014). We identified specific expression of the antiviral gene IFITM3
511 in CTB 4. IFITM3 expression is particularly interesting due to the recent finding that it blocks
512 STB fusion mediated by the endogenous retroviral elements, ERVW-1 and ERVFRD-1.
513 Therefore, IFITM3 expression in SC-CTBs may have a dual role – restricting viral entry into the
514 cell and blocking the formation of STBs in the SC. Its expression also provides a mechanism by
515 which the lack of STBs in the smooth chorion is maintained after degradation of the villi is
516 complete.
517
518 A distinct feature of the CTBs of the SC was remodeling of the cytokeratin network coordinated
519 with differentiation from CTB 1 to SC-CTBs. The progressive expression of KRT14, KRT17, and
520 KRT6A is reminiscent of the cytokeratin code found in the epithelial cell layers of many tissues
521 (Karantza et al., 2011). KRT14 is recognized as a marker of all stratified epithelium including
522 subsets of basal progenitor and stem cells in several tissues, usually alongside KRT5 (Moll et
523 al., 1982; Nelson et al., 1983; Rock et al., 2009). While we did not identify expression of KRT5
524 in any trophoblast, the KRT14 expressing proliferative cells of the SC fit the profile of stratified
525 epithelia in other locations. The roles of KRT17 and KRT6 are less clear. Most knowledge about
526 the function of these molecules comes from the epidermis in the context of injury and disease.
527 KRT6 and KRT17 are upregulated rapidly upon epidermal injury and are expressed through the
528 repair phase, each contributing specific functions. (Takahashi et al., 1998; McGowan and
529 Coulombe, 1998). KRT17 promotes proliferation and increases in cell size through Akt/mTOR
530 and STAT3, respectively (Kim et al., 2006; Yang et al., 2018). KRT6 is a negative regulator of
531 cell migration through the inhibition of Src kinase and associations with myosinIIA (Wong and
532 Coulombe, 2003; Rotty and Coulombe, 2012; Wang et al., 2018). Finally, this molecule promotes
533 expression of Desmoplakin and the maintenance of desmosomes, the latter, a long-established
534 feature of SC trophoblasts (Bou-Resli et al., 1981; Bartels and Wang, 1983; Benirschke et al.,
535 2006). Taken together, these observations are consistent with data on SC-CTBs. We found no
536 evidence of their invasion, but did identify frequent interactions with the ECM, CTBs, and EVTs.

537 The coordinated expression of these cytokeratins and the transcriptional profile writ large,
538 suggested the SC has the properties of a highly specialized epidermis with a robust proliferative
539 capacity and strong cohesive properties, but lacking migratory or invasive behavior.
540
541 As previous work has demonstrated or assumed, the majority of trophoblast identified are
542 represented in both the VC and SC (Benirschke et al., 2006; Garrido-Gomez et al., 2017; Pique-
543 Regi et al., 2019). We identified two cell types with striking transcriptional similarity between
544 regions, CTB 1 and EVT. CTB 1 cells in the VC matched canonical villous CTB in transcriptional
545 profile, behavior, and niche. Surprisingly, we identified a similar population in the SC. They are
546 localized to an epithelial sheet juxtaposed to the fetal mesenchyme, separated by a thin basal
547 lamina. These cells are supported by similar signaling pathways in both regions, including HGF
548 and WNT (Figure 1-S3g; Dokras et al., 2001; Okae et al., 2018; Zhou et al., 2002). The
549 similarities in location and growth factor requirements demonstrate that a niche similar to the
550 villous trophoblast membrane, exists in the SC. Additionally, we identified CTB 1 as the
551 progenitor population for SC-CTB, and possibly for EVT in the SC. Thus, CTB 1 in both regions
552 function as multipotent progenitors. Despite the many similarities, the developmental trajectories
553 emerging from CTB 1 differ in a region-specific manner. At present, it is unclear whether CTB 1
554 cells in both regions originally have the same potential or if fate restriction occurs as the fetal
555 membranes form. Future experiments will need to functionally address whether CTB 1 from the
556 VC can be coerced to generate SC-CTBs and if CTB 1 from the SC can efficiently generate
557 STBs and invasive EVTs. Multipotent trophoblasts have been generated from first trimester
558 smooth chorion cells, however, these cells have a distinct transcriptional profile from the second
559 trimester cells we characterized (Genbacev et al., 2016).
560
561 Similarities between the EVT of each region, as defined by contact with the decidua, has been
562 documented in observational, molecular, and most recently, transcriptomic studies (Benirschke
563 et al., 2006, Pique-Regi et al., 2019). Our data confirmed a strong correlation between gene
564 expression for all EVT populations, regardless of regional identity. Based on previously
565 established EVT subtypes, we identified a reduction in the proportion of interstitial EVTs and a
566 concomitant increase in columnar-like EVTs of the SC. However, we did not find evidence of
567 specific EVT subpopulations or intrinsic gene expression programs that would explain the
568 differences in the depth of invasion of EVT in each placental region. However, we did uncover
569 CTB-EVT interactions specific to the SC epithelium. Rather than physically separating as they
570 do in the VC, CTBs and EVTs co-occupy the stratified epithelium of the SC, providing a
571 contained environment for paracrine signaling, cell contact mediated signaling, and cell-ECM
572 interactions that may impact trophoblast invasion. In this study we verified that soluble signaling
573 factors from SC cells restrict the invasion of their counterparts from the VC. We can speculate
574 on potential candidates that may function across multiple biological systems to restrict invasion.
575 CTB 4 cells express high levels of TIMP1, TIMP3, and SERPINE1 (PAI-1), which inhibit the
576 function and/or activation of MMPs necessary for trophoblast invasion (Fisher et al., 1989; Zhu
577 et al., 2012). Addition of recombinant TIMPs or a function blocking antibody against plasminogen
578 (whose processing is inhibited by SERPINE1) reduced trophoblast invasion *in vitro* (Lala and
579 Graham, 1990). While these molecules are expressed by decidual cells, we identified their
580 expression within the SC epithelium directly adjacent to EVTs. Another candidate regulator of

581 invasion expressed by CTB 4 is TNFα. Treatment of trophoblasts with TNFα increases EVT
582 apoptosis, decreases protease expression, increases SERPINE1 expression, and decreases
583 invasion *in vitro* (Otun et al., 2011; Xu et al., 2011). These data suggest that SC-CTBs secrete
584 multiple molecules that could decrease the survival and invasion of EVTs in the SC. In this study
585 we explored the role of secreted factors, but SC-CTBs may also influence EVTs through cell
586 contact mediated signaling and the deposition of an ECM distinct from the basal plate. Future
587 experiments will be necessary to explore the contributions of these distinct signaling pathways
588 and matrices.
589
590 In summary, this study provides a high-resolution molecular accounting of the trophoblast that
591 occupy smooth chorion. By comparison with trophoblasts isolated from the VC of the same
592 placentas, we identified key similarities and differences to better understand the molecular
593 determinants of trophoblast function and behavior in the SC. We characterized a novel CTB
594 population, marked by KRT6A expression, that is central to three key functions of the SC:
595 formation of an epidermal-like barrier, blockage of aberrant STB differentiation, and restriction
596 of EVT invasion. These data provide a better understanding of molecular and cellular pathways
597 that control human placental development and against which disease related changes can be
598 identified and therapeutic targets discovered.

599 **Key Resources Table**

Reagent type (species) or resource	Designation	Source or reference	Identifiers	Additional information
Antibody	Rat anti E-cadherin Monoclonal Antibody (ECCD-2)	Thermofisher Scientific	13-1900	IF (1:250)
Antibody	Rabbit Anti-PAGE4 antibody (Polyclonal)	Sigma Aldrich	HPA023880	IF (1:100)
Antibody	Rabbit Recombinant Anti-Cytokeratin 6 Monoclonal antibody [EPR1603Y]	Abcam	ab52620	IF (1:100)
Antibody	Rabbit anti Non-phospho (Active) β-Catenin (Ser33/37/Thr41) Monoclonal Antibody	Cell Signaling	8814	IF (1:100)
Antibody	Mouse anti Cytokeratin 14 Monoclonal Antibody (LL002)	Invitrogen	MA5-11599	IF (1:100) with Antigen Retrieval
Antibody	Rabbit Anti-KLF4 antibody (polyclonal)	Sigma Aldrich	HPA00292	IF (1:100)
Antibody	Cytokeratin (7D3) Monoclonal Antibody	Susan Fisher/University of California, San Francisco Cat# Fisher_001-clone7D3,RRID:AB_2631235 https://antibodyregistry.org/search?q=AB2631235	AB_2631235	IF (1:100)
Antibody	HLA-G (4H84) Monoclonal Antibody	Susan Fisher/University of California, San Francisco Cat# Fisher_002-clone4H84, RRID:AB_2631236 https://antibodyregistry.org/search?q=AB2631236	AB_2631236	IF (1:20) with Antigen Retrieval
Software, algorithm	R	https://www.r-project.org/		
Software, algorithm	ImageJ	ImageJ (http://imagej.nih.gov/ij/)		
Software, algorithm	Seurat (3.1.3)	https://satijalab.org/seurat/		
Software, algorithm	cellranger (3.0.2)	https://support.10xgenomics.com/single-cell-gene-expression/software/pipelines/latest/feature-bc		
Software, algorithm	ClusterProfiler	https://guangchuangyu.github.io/software/clusterProfiler/		
Software, algorithm	scVelo	https://github.com/theislab/scvelo		
Software, algorithm	Prism 6.0	https://www.graphpad.com/scientific-software/prism/		
Software, algorithm	DoubletFinder	https://github.com/chris-mcginnis-ucsf/DoubletFinder		

600
601

Methods

Cellular Isolation of VC trophoblast: Trophoblast were isolated from both floating and anchoring villi dissected from 2nd trimester human placentas. Trophoblast were isolated according to previously published protocols (Fisher et al., 1989; Kliman and Feinberg, 1990).

Cellular Isolation of SC trophoblast: Trophoblast were isolated according to previously published protocols (Garrido-Gomez et al., 2017).

Single Cell RNA-Sequencing and Analysis: To capture the transcriptome of individual cells we used the Chromium Single Cell 3' Reagent V3 Kit from 10X Genomics. For all samples 17,500 cells were loaded into one well of a Chip B kit for GEM generation. Library preparation including, reverse transcription, barcoding, cDNA amplification, and purification was performed according to Chromium 10x V3 protocols. Each sample was sequenced on a NovaSeq 6000 S4 to a depth of approximately 20,000-30,000 reads per cell. The gene expression matrices for each dataset was generated using the CellRanger software (v3.0.2 - 10x Genomics). All reads were aligned to GRCh38 using STAR. (https://support.10xgenomics.com/single-cell-gene-expression/software/pipelines/latest/advanced/references). The counts matrix was thresholded and analyzed in the package Seurat (v3.1.3). Cells with fewer than 500 or greater than 6000 unique genes, as well as all cells with greater than 15 percent mitochondrial counts, were excluded from all subsequent analyses. Doublet detection was performed for each sample using DoubletFinder and all doublets were excluded from analysis. For each sample, counts were scaled and normalized using ScaleData and NormalizeData, respectively, with default settings FindVariableFeatures used to identify the 2000 most variable genes as input for all future analyses. PCA was performed using RunPCA and significant PCs assessed using ElbowPlot and DimHeatmap. Dimensionality reduction and visualization using UMAP was performed by RunUMAP.

Integration of each timepoint into one dataset was performed using FindIntegrationAnchors and IntegrateData, both using 20 dimensions (after filtering each dataset for number of genes, mitochondrial counts, and normalizing as described above). Data scaling, PCA, selection of PCs, clustering and visualization proceeded as described above using 30 PCs and a resolution of 0.6.

To generate the trophoblast, stroma, and immune cell subsets, the respective clusters were subset from the integrated dataset using the function SubsetData based upon annotations from marker genes identified by FindAllMarkers. After subsetting, counts were scaled and normalized using ScaleData and NormalizeData, respectively, with default settings FindVariableFeatures used to identify the 2000 most variable genes. Differentially expressed genes for each integrated dataset were identified using FindAllMarkers.

scVelo: RNA velocity analysis was applied to the entire conglomerate dataset using Velocyto to generate spliced and unspliced reads for all cells. This dataset was then subset for the trophoblast dataset introduced in Figure 2. The scVelo dynamical model was run with default settings and subset by each timepoint.

646
647 **Differential expression between regions:** The number of trophoblast cells in each cluster were
648 downsampled to 100 cells from each region of origin and performed differential expression using
649 FindMarkers function and repeated this for 100 permutations. The number of genes found to be
650 significantly differentially expressed (adj. P-value <0.05) from each permutation are plotted.
651 Clusters having less that 100 cells from each region were excluded from this analysis.
652
653 **Gene Ontology Analysis:** Gene Ontology analysis was performed with ClusterProfiler
654 enrichGO function. The simplify function within this package was used to consolidate
655 hierarchically related terms using a cutoff of 0.5. Terms were considered significantly enriched
656 with an adjusted P-value of less than 0.05.
657
658 **Immunofluorescence Staining:** Placental tissue for cryosectioning was fixed in 3% PFA at 4°C
659 for 8hrs, washed in 1x PBS, then submerged in 30% sucrose overnight at 4°C prior to embedding
660 in OCT medium. Placental tissue in OCT was sectioned at 5μm for all conditions. In brief, slides
661 were washed in 1x PBST (1x PBS, 0.05% Tween-20), blocked for 1hr (1x PBS + 5% donkey or
662 goat serum + 0.3% TritonX), incubated in primary antibody diluted for 3 hours at room
663 temperature (or overnight at 4°C), washed in 1x PBST, incubated in secondary antibody
664 (Alexafluor 488 or 594) for 1 hour at room temperature, incubated in DAPI for 10min at room
665 temp, washed in 1x PBST, and mounted and sealed for imaging. Any antigen retrieval was
666 performed prior to the blocking step by heating the slides in a 1x citrate buffer with 0.05% Tween-
667 20 at 95C for 30 minutes. All antibodies and the dilutions are listed in the key resources table.
668 All immunofluorescence staining was performed in n=3 biological replicates (3 distinct placentas)
669 and representative image is shown.
670
671 **Transwell Invasion Assay:** 24-well plate transwell inserts with an 8 μM polycarbonate
672 membrane (Corning Costar 3422) were coated with 10μL of Matrigel (growth factor-containing,
673 Corning Corp, USA) diluted 1:1 in Serum Free Media (95% DME H-21 + Glutamine, 2%
674 Nutridoma (mostly β-D xylopyranose), 1% Pen Strep, 1% Hepes, 0.1% Gentamycin). Cells from
675 each region of the placenta were isolated as described above and then plated in the upper well
676 of the transwell insert at a density of 250,000 cells in 250μL of Serum Free Media, with 1mL of
677 Serum Free Media (or conditioned media) in the well below the insert. The cells were then
678 cultured for 39 hours. The cells in the transwell were then fixed in 3% PFA for 10min at 4C,
679 permeabilized in ice cold methanol for 10min at 4C, then washed in 1x PBS, incubated in Pan-
680 CK primary antibody for 3 hours at 37C, washed in 1x PBS, incubated with secondary antibody
681 (Alexafluor 594) and DAPI for 1 hour at 37C, washed in 1x PBS, then mounted and sealed for
682 imaging.
683
684 **Transwell Invasion Assay Quantification:** Transwell membranes mounted on slides were
685 imaged at 40x magnification and the number of Pan-CK positive projections through the
686 membrane counted. Normalization for changes in cell density across fields of view and culture
687 conditions was performed by quantifying the DAPI positive area of each image and the number
688 of projections normalized to the median across comparisons.
689

690 **Culture of placental cells and generation of conditioned media:** Each well of a 24-well plate
691 was coated with 20μL of Matrigel undiluted (growth factor-containing, Corning Corp, USA) prior
692 to cell seeding. Cells from each region of the placenta were isolated as described above and
693 then plated into wells of a 24-well plate at a density of $1x10^6$ cells in 1mL of Serum Free Media
694 (95% DME H-21 + Glutamine, 2% Nutridoma (mostly β-D xylopyranose), 1% Pen Strep, 1%
695 Hepes, 0.1% Gentamycin). The cells were cultured for 39 hours. After 39 hours in culture the
696 media was removed and centrifuged at 2000g for 10mins to remove cellular debris. The
697 supernatant was then removed, snap frozen in LN2, and stored at -80C. This media was then
698 thawed and used as conditioned media.

Data Availability

All sequencing data is available at the NCBI Gene Expression Omnibus GSE198373. Processed data are available as R objects at https://figshare.com/projects/Regionally_distinct_trophoblast_regulate_barrier_function_and_invasion_in_the_human_placenta/135191.

Acknowledgements

We thank the members of the University of California – San Francisco National Center of Translational Research in Reproduction and Infertility for helpful comments during the design, execution, and publication of this project. We would also like to thank all members of the Blelloch and Fisher Labs for their comments and support. We specifically thank Ali San and Nasim Zeighami for their research contributions. We would also like to acknowledge our funding sources, the NIH Eunice Kennedy Shriver National Institute for Child Health and Human Development P50 HD055764 and NIH R37 HD076253.

Competing Interests

Susan Fisher is a consultant for Novo Nordisk. All other authors declare no competing interests.

716 **References**

717 Baczyk, D., Drewlo, S., Proctor, L., Dunk, C., Lye, S., & Kingdom, J. (2009). Glial cell missing-
718 1 transcription factor is required for the differentiation of the human trophoblast. *Cell Death*
719 *and Differentiation*, *16*(5), 719–727. https://doi.org/10.1038/cdd.2009.1

720 Bailey, C. C., Zhong, G., Huang, I. C., & Farzan, M. (2014). IFITM-family proteins: The cell's
721 first line of antiviral defense. *Annual Review of Virology*, *1*(1), 261–283.
722 https://doi.org/10.1146/annurev-virology-031413-085537

723 Bartles, H., & Wang, T. (1983). Intercellular Junctions in the Human Fetal Membranes.
724 *Anatomy and Embryology*, 103–120.

725 Benirschke, K., Kaufmann, P., & Baergen, R. (2006). Pathology of the Human Placenta. In
726 *Pathology* (Vol. 38, Issue 2). https://doi.org/10.1016/s0031-3025(16)39684-2

727 Bergen, V., Lange, M., Peidli, S., Wolf, F. A., & Theis, F. J. (2020). Generalizing RNA velocity
728 to transient cell states through dynamical modeling. *Nature Biotechnology*, *38*(12), 1408–
729 1414. https://doi.org/10.1038/s41587-020-0591-3

730 Blaise, S., De Parseval, N., Bénit, L., & Heidmann, T. (2003). Genome wide screening for
731 fusogenic human endogenous retrovirus envelopes identifies syncytin 2, a gene
732 conserved on primate evolution. *Proceedings of the National Academy of Sciences of the*
733 *United States of America*, *100*(22), 13013–13018.
734 https://doi.org/10.1073/pnas.2132646100

735 Boyd, J. D., & Hamilton, W. J. (1967). Development and Structure of the Human Placenta
736 From the End of the 3Rd Month of Gestation. *BJOG: An International Journal of Obstetrics*
737 *& Gynaecology*, *74*(2), 161–226. https://doi.org/10.1111/j.1471-0528.1967.tb14864.x

738 Buchrieser, J., Degrelle, S. A., Couderc, T., Nevers, Q., Disson, O., Manet, C., Donahue, D.
739 A., Porrot, F., Hillion, K. H., Perthame, E., Arroyo, M. V., Souquere, S., Ruigrok, K.,
740 Dupressoir, A., Heidmann, T., Montagutelli, X., Fournier, T., Lecuit, M., & Schwartz, O.
741 (2019). IFITM proteins inhibit placental syncytiotrophoblast formation and promote fetal
742 demise. *Science*, *365*(6449), 176–180. https://doi.org/10.1126/science.aaw7733

743 Del Peso, L., Castellanos, M. C., Temes, E., Martín-Puig, S., Cuevas, Y., Olmos, G., &
744 Landázuri, M. O. (2003). The von Hippel Lindau/hypoxia-inducible factor (HIF) pathway
745 regulates the transcription of the HIF-proline hydroxylase genes in response to low
746 oxygen. *Journal of Biological Chemistry*, *278*(49), 48690–48695.
747 https://doi.org/10.1074/jbc.M308862200

748 Dokras, A., Gardner, L. M. G., Seftor, E. A., & Hendrix, M. J. C. (2001). Regulation of human
749 cytotrophoblast morphogenesis by hepatocyte growth factor/scatter factor. *Biology of*
750 *Reproduction*, *65*(4), 1278–1288. https://doi.org/10.1095/biolreprod65.4.1278

751 Ferreira, L. M. R., Meissner, T. B., Mikkelsen, T. S., Mallard, W., O'Donnell, C. W., Tilburgs, T.,
752 Gomes, H. A. B., Camahort, R., Sherwood, R. I., Gifford, D. K., Rinn, J. L., Cowan, C. A.,
753 & Strominger, J. L. (2016). A distant trophoblast-specific enhancer controls HLA-G
754 expression at the maternal-fetal interface. *Proceedings of the National Academy of*

Sciences of the United States of America, *113*(19), 5364–5369. https://doi.org/10.1073/pnas.1602886113

Fisher, S. J., Cui, T., Zhang, L., Hartman, L., Grahl, K., Guo-Yang, Z., Tarpey, J., & Damsky, C. H. (1989). Adhesive and degradative properties of human placental cytotrophoblast cells in vitro. *Journal of Cell Biology*, *109*(2), 891–902. https://doi.org/10.1083/jcb.109.2.891

Garrido-Gomez, T., Ona, K., Kapidzic, M., Gormley, M., Simón, C., Genbacev, O., & Fisher, S. J. (2017). Severe pre-eclampsia is associated with alterations in cytotrophoblasts of the smooth chorion. In *Development (Cambridge)* (Vol. 144, Issue 5, pp. 767–777). https://doi.org/10.1242/dev.146100

Genbacev, O., Larocque, N., Ona, K., Prakobphol, A., Garrido-Gomez, T., Kapidzic, M., Bárcena, A., Gormley, M., & Fisher, S. J. (2016). Integrin α4-positive human trophoblast progenitors: Functional characterization and transcriptional regulation. *Human Reproduction*, *31*(6), 1300–1314. https://doi.org/10.1093/humrep/dew077

Genbačev, O., Vićovac, L., & Larocque, N. (2015). The role of chorionic cytotrophoblasts in the smooth chorion fusion with parietal decidua. In *Placenta* (Vol. 36, Issue 7, pp. 716–722). https://doi.org/10.1016/j.placenta.2015.05.002

Genbacev, O., Zhou, Y., Ludlow, J. W., & Fisher, S. J. (1997). Regulation of human placental development by oxygen tension. *Science*, *277*(5332), 1669–1672. https://doi.org/10.1126/science.277.5332.1669

Haider, S., Meinhardt, G., Saleh, L., Kunihs, V., Gamperl, M., Kaindl, U., Ellinger, A., Burkard, T. R., Fiala, C., Pollheimer, J., Mendjan, S., Latos, P. A., & Knöfler, M. (2018). Self-Renewing Trophoblast Organoids Recapitulate the Developmental Program of the Early Human Placenta. *Stem Cell Reports*, *11*(2), 537–551. https://doi.org/10.1016/j.stemcr.2018.07.004

Hamilton, W. J., & Boyd, J. D. (1960). Development of the human placenta in the first three months of gestation. *Journal of Anatomy*, *94*, 297–328. http://www.ncbi.nlm.nih.gov/pubmed/14399291%0Ahttp://www.pubmedcentral.nih.gov/articlerender.fcgi?artid=PMC1244370

Harris, L. K., Jones, C. J. P., & Aplin, J. D. (2009). Adhesion Molecules in Human Trophoblast - A Review. II. Extravillous Trophoblast. *Placenta*, *30*(4), 299–304. https://doi.org/10.1016/j.placenta.2008.12.003

Harvey, K. F., Zhang, X., & Thomas, D. M. (2013). The Hippo pathway and human cancer. *Nature Reviews Cancer*, *13*(4), 246–257. https://doi.org/10.1038/nrc3458

Karantza, V. (2011). Keratins in health and cancer: More than mere epithelial cell markers. *Oncogene*, *30*(2), 127–138. https://doi.org/10.1038/onc.2010.456

Kliman, H. J., & Feinbergt, R. F. (1990). Human trophoblast-extracellular matrix (ECM) interactions in vitro: ECM thickness modulates morphology and proteolytic activity (invasion/placenta/choriocarcinoma/Matrigel/cyclic AMP). *Proc. Nat. Acad. Sci. USA*, *87*(April), 3057–3061.

795 Knöfler, M., Haider, S., Saleh, L., Pollheimer, J., Gamage, T. K. J. B., & James, J. (2019).
796 Human placenta and trophoblast development: key molecular mechanisms and model
797 systems. In *Cellular and Molecular Life Sciences*. https://doi.org/10.1007/s00018-019-
798 03104-6

799 Lala, P. K., & Graham, C. H. (1990). Mechanisms of trophoblast invasiveness and their control:
800 the role of proteases and protease inhibitors. *Cancer and Metastasis Review*, *9*(4), 369–
801 379. https://doi.org/10.1007/BF00049525

802 Lee, C. Q. E., Gardner, L., Turco, M., Zhao, N., Murray, M. J., Coleman, N., Rossant, J.,
803 Hemberger, M., & Moffett, A. (2016). What Is Trophoblast? A Combination of Criteria
804 Define Human First-Trimester Trophoblast. *Stem Cell Reports*, *6*(2), 257–272.
805 https://doi.org/10.1016/j.stemcr.2016.01.006

806 Liu, X.-Y., Chen, W., Wei, B., Shan, Y.-F., & Wang, C. (2011). IFN-Induced TPR Protein IFIT3
807 Potentiates Antiviral Signaling by Bridging MAVS and TBK1. *The Journal of Immunology*,
808 *187*(5), 2559–2568. https://doi.org/10.4049/jimmunol.1100963

809 Liu, Y., Fan, X., Wang, R., Lu, X., Dang, Y. L., Wang, H., Lin, H. Y., Zhu, C., Ge, H., Cross, J.
810 C., & Wang, H. (2018). Single-cell RNA-seq reveals the diversity of trophoblast subtypes
811 and patterns of differentiation in the human placenta. *Cell Research*.
812 https://doi.org/10.1038/s41422-018-0066-y

813 Lu, X., Wang, R., Zhu, C., Wang, H., Lin, H. Y., Gu, Y., Cross, J. C., & Wang, H. (2017). Fine-
814 Tuned and Cell-Cycle-Restricted Expression of Fusogenic Protein Syncytin-2 Maintains
815 Functional Placental Syncytia. *Cell Reports*, *21*(5), 1150–1159.
816 https://doi.org/10.1016/j.celrep.2017.10.019

817 Maxwell, P. H., Dachs, G. U., Gleadle, J. M., Nicholls, L. G., Harris, A. L., Stratford, I. J.,
818 Hankinson, O., Pugh, C. W., & Ratcliffe, P. J. (1997). Hypoxia-inducible factor-1
819 modulates gene expression in solid tumors and influences both angiogenesis and tumor
820 growth. *Proceedings of the National Academy of Sciences of the United States of*
821 *America*, *94*(15), 8104–8109. https://doi.org/10.1073/pnas.94.15.8104

822 McGinnis, C. S., Murrow, L. M., & Gartner, Z. J. (2019). DoubletFinder: Doublet Detection in
823 Single-Cell RNA Sequencing Data Using Artificial Nearest Neighbors. *Cell Systems*, *8*(4),
824 329-337.e4. https://doi.org/10.1016/j.cels.2019.03.003

825 McGowan, K. M., & Coulombe, P. A. (1998). Onset of keratin 17 expression coincides with the
826 definition of major epithelial lineages during skin development. *Journal of Cell Biology*,
827 *143*(2), 469–486. https://doi.org/10.1083/jcb.143.2.469

828 McMaster, M. T., Librach, C. L., Zhou, Y., Lim, K. H., Janatpour, M. J., DeMars, R., Kovats, S.,
829 Damsky, C., & Fisher, S. J. (1995). Human placental HLA-G expression is restricted to
830 differentiated cytotrophoblasts. *Journal of Immunology (Baltimore, Md. : 1950)*, *154*(8),
831 3771–3778. http://www.ncbi.nlm.nih.gov/pubmed/7706718

832 Mi, S. (2000). *Syncytin is a captive retrovirus*. *403*(February), 785–789. www.nature.com

833 Moll, R., Franke, W. W., Schiller, D. L., Geiger, B., & Krepler, R. (1982). The catalog of human
834 cytokeratins: Patterns of expression in normal epithelia, tumors and cultured cells. *Cell*,
835 *31*(1), 11–24. https://doi.org/10.1016/0092-8674(82)90400-7

836 Nelson, W. G., & Sun, T. T. (1983). The 50- and 58-kdalton keratin classes as molecular
837 markers for stratified squamous epithelia: Cell culture studies. *Journal of Cell Biology*,
838 *97*(1), 244–251. https://doi.org/10.1083/jcb.97.1.244

839 Okae, H., Toh, H., Sato, T., Hiura, H., Takahashi, S., Shirane, K., Kabayama, Y., Suyama, M.,
840 Sasaki, H., & Arima, T. (2018). Derivation of Human Trophoblast Stem Cells. *Cell Stem*
841 *Cell*, *22*(1), 50-63.e6. https://doi.org/10.1016/j.stem.2017.11.004

842 Otun, H. A., Lash, G. E., Innes, B. A., Bulmer, J. N., Naruse, K., Hannon, T., Searle, R. F., &
843 Robson, S. C. (2011). Effect of tumour necrosis factor-α in combination with interferon-γ
844 on first trimester extravillous trophoblast invasion. *Journal of Reproductive Immunology*,
845 *88*(1), 1–11. https://doi.org/10.1016/j.jri.2010.10.003

846 Parry, S., & Strauss, J. (1998). Premature rupture of the fetal membranes. *The New England*
847 *Journal of Medicine*, *338*(10), 663–670.

848 Red-Horse, K., Zhou, Y., Genbacev, O., Prakobphol, A., Foulk, R., McMaster, M., & Fisher, S.
849 J. (2004). Trophoblast differentiation during embryo implantation and formation of the
850 maternal-fetal interface. *The Journal of Clinical Investigation*, *114*(6), 744–754.
851 https://doi.org/10.1172/JCI22991

852 Rock, J. R., Gao, X., Xue, Y., Randell, S. H., Kong, Y. Y., & Hogan, B. L. M. (2011). Notch-
853 dependent differentiation of adult airway basal stem cells. *Cell Stem Cell*, *8*(6), 639–648.
854 https://doi.org/10.1016/j.stem.2011.04.003

855 Rock, J. R., Onaitis, M. W., Rawlins, E. L., Lu, Y., Clark, C. P., Xue, Y., Randell, S. H., &
856 Hogan, B. L. M. (2009). Basal cells as stem cells of the mouse trachea and human airway
857 epithelium. *Proceedings of the National Academy of Sciences of the United States of*
858 *America*, *106*(31), 12771–12775. https://doi.org/10.1073/pnas.0906850106

859 Romero, R., Dey, S. K., & Fisher, S. J. (2014). Preterm labor: One syndrome, many causes.
860 *Science*, *345*(6198), 760–765. https://doi.org/10.1126/science.1251816

861 Rotty, J. D., & Coulombe, P. A. (2012). A wound-induced keratin inhibits Src activity during
862 keratinocyte migration and tissue repair. *Journal of Cell Biology*, *197*(3), 381–389.
863 https://doi.org/10.1083/jcb.201107078

864 Segre, J. A., Bauer, C., & Fuchs, E. (1999). Klf4 is a transcription factor required for
865 establishing the barrier function of the skin. *Nature Genetics*, *22*(4), 356–360.
866 https://doi.org/10.1038/11926

867 Spence, J. S., He, R., Hoffmann, H. H., Das, T., Thinon, E., Rice, C. M., Peng, T., Chandran,
868 K., & Hang, H. C. (2019). IFITM3 directly engages and shuttles incoming virus particles to
869 lysosomes. *Nature Chemical Biology*, *15*(3), 259–268. https://doi.org/10.1038/s41589-
870 018-0213-2

871 Stuart, T., Butler, A., Hoffman, P., Hafemeister, C., Papalexi, E., Mauck, W. M., Hao, Y.,
872 Stoeckius, M., Smibert, P., & Satija, R. (2019). Comprehensive Integration of Single-Cell
873 Data. *Cell*, *177*(7), 1888-1902.e21. https://doi.org/10.1016/j.cell.2019.05.031

874 Suryawanshi, H., Morozov, P., Straus, A., Sahasrabudhe, N., Max, K. E. A., Garzia, A.,
875 Kustagi, M., Tuschl, T., & Williams, Z. (2018). A single-cell survey of the human first-
876 trimester placenta and decidua. *Science Advances*.
877 https://doi.org/10.1126/sciadv.aau4788

878 Takahashi, K., Yan, B., Yamanishi, K., Imamura, S., & Coulombe, P. A. (1998). The two
879 functional keratin 6 genes of mouse are differentially regulated and evolved independently
880 from their human orthologs. *Genomics*, *53*(2), 170–183.
881 https://doi.org/10.1006/geno.1998.5476

882 Thurman, J. M., & Holers, V. M. (2006). The Central Role of the Alternative Complement
883 Pathway in Human Disease. *The Journal of Immunology*, *176*(3), 1305–1310.
884 https://doi.org/10.4049/jimmunol.176.3.1305

885 Tilburgs, T., Crespo, Â. C., Van Der Zwan, A., Rybalov, B., Raj, T., Stranger, B., Gardner, L.,
886 Moffett, A., & Strominger, J. L. (2015). Human HLA-G+ extravillous trophoblasts: Immune-
887 activating cells that interact with decidual leukocytes. *Proceedings of the National*
888 *Academy of Sciences of the United States of America*, *112*(23), 7219–7224.
889 https://doi.org/10.1073/pnas.1507977112

890 Tirosh, I., Izar, B., Prakadan, S. M., Wadsworth, M. H., Treacy, D., Trombetta, J. J., Rotem, A.,
891 Rodman, C., Lian, C., Murphy, G., Fallahi-Sichani, M., Dutton-Regester, K., Lin, J. R.,
892 Cohen, O., Shah, P., Lu, D., Genshaft, A. S., Hughes, T. K., Ziegler, C. G. K., …
893 Garraway, L. A. (2016). Dissecting the multicellular ecosystem of metastatic melanoma by
894 single-cell RNA-seq. *Science*, *352*(6282), 189–196.
895 https://doi.org/10.1126/science.aad0501

896 Vento-Tormo, R., Efremova, M., Botting, R. A., Turco, M. Y., Vento-Tormo, M., Meyer, K. B.,
897 Park, J. E., Stephenson, E., Polański, K., Goncalves, A., Gardner, L., Holmqvist, S.,
898 Henriksson, J., Zou, A., Sharkey, A. M., Millar, B., Innes, B., Wood, L., Wilbrey-Clark, A.,
899 … Teichmann, S. A. (2018). Single-cell reconstruction of the early maternal–fetal interface
900 in humans. *Nature*. https://doi.org/10.1038/s41586-018-0698-6

901 Wang, F., Chen, S., Liu, H. B., Parent, C. A., & Coulombe, P. A. (2018). Keratin 6 regulates
902 collective keratinocyte migration by altering cell–cell and cell–matrix adhesion. *Journal of*
903 *Cell Biology*, *217*(12), 4314–4330. https://doi.org/10.1083/jcb.201712130

904 Wong, P., & Coulombe, P. A. (2003). Loss of keratin 6 (K6) proteins reveals a function for
905 intermediate filaments during wound repair. *Journal of Cell Biology*, *163*(2), 327–337.
906 https://doi.org/10.1083/jcb.200305032

907 Xu, B., Nakhla, S., Makris, A., & Hennessy, A. (2011). TNF-α inhibits trophoblast integration
908 into endothelial cellular networks. *Placenta*, *32*(3), 241–246.
909 https://doi.org/10.1016/j.placenta.2010.12.005

910 Yabe, S., Alexenko, A. P., Amita, M., Yang, Y., Schust, D. J., Sadovsky, Y., Ezashi, T., &
911 Roberts, R. M. (2016). Comparison of syncytiotrophoblast generated from human

embryonic stem cells and from term placentas. *Proceedings of the National Academy of Sciences of the United States of America*, *113*(19), E2598–E2607. https://doi.org/10.1073/pnas.1601630113

Yang, L., Jin, L., Ke, Y., Fan, X., Zhang, T., Zhang, C., Bian, H., & Wang, G. (2018). E3 Ligase Trim21 Ubiquitylates and Stabilizes Keratin 17 to Induce STAT3 Activation in Psoriasis. *Journal of Investigative Dermatology*, *138*(12), 2568–2577. https://doi.org/10.1016/j.jid.2018.05.016

Yeh, I. T., O'Connor, D. M., & Kurman, R. J. (1989). Vacuolated Cytotrophoblast: A subpopulation of trophoblast in the chorion laeve. *Placenta*, *10*(5), 429–438. https://doi.org/10.1016/0143-4004(89)90053-2

Yu, G., Wang, L. G., Han, Y., & He, Q. Y. (2012). ClusterProfiler: An R package for comparing biological themes among gene clusters. *OMICS A Journal of Integrative Biology*, *16*(5), 284–287. https://doi.org/10.1089/omi.2011.0118

Yuan, B., Ohyama, K., Bessho, T., & Toyoda, H. (2006). Contribution of inducible nitric oxide synthase and cyclooxygenase-2 to apoptosis induction in smooth chorion trophoblast cells of human fetal membrane tissues. *Biochemical and Biophysical Research Communications*, *341*(3), 822–827. https://doi.org/10.1016/j.bbrc.2006.01.042

Yuan, B., Ohyama, K., Bessho, T., Uchide, N., & Toyoda, H. (2008). Imbalance between ROS production and elimination results in apoptosis induction in primary smooth chorion trophoblast cells prepared from human fetal membrane tissues. *Life Sciences*, *82*(11–12), 623–630. https://doi.org/10.1016/j.lfs.2007.12.016

Yuan, B., Ohyama, K., Takeichi, M., & Toyoda, H. (2009). Direct contribution of inducible nitric oxide synthase expression to apoptosis induction in primary smooth chorion trophoblast cells of human fetal membrane tissues. *International Journal of Biochemistry and Cell Biology*, *41*(5), 1062–1069. https://doi.org/10.1016/j.biocel.2008.09.031

Zhou, Y., McMaster, M., Woo, K., Janatpour, M., Perry, J., Karpanen, T., Alitalo, K., Damsky, C., & Fisher, S. J. (2002). Vascular endothelial growth factor ligands and receptors that regulate human cytotrophoblast survival are dysregulated in severe preeclampsia and hemolysis, elevated liver enzymes, and low platelets syndrome. *American Journal of Pathology*, *160*(4), 1405–1423. https://doi.org/10.1016/S0002-9440(10)62567-9

Zhu, J.-Y., Pang, Z.-J., & Yu, Y.-H. (2012). Regulation of trophoblast invasion: the role of matrix metalloproteinases. *Reviews in Obstetrics & Gynecology*, *5*(3–4), e137-43. https://doi.org/10.3909/riog0196

946 **Supplementary Tables**

947

948 Supplementary Table 1 - Number of cells captured from each region per cluster for the
949 trophoblast dataset.

950

Supplementary Figures

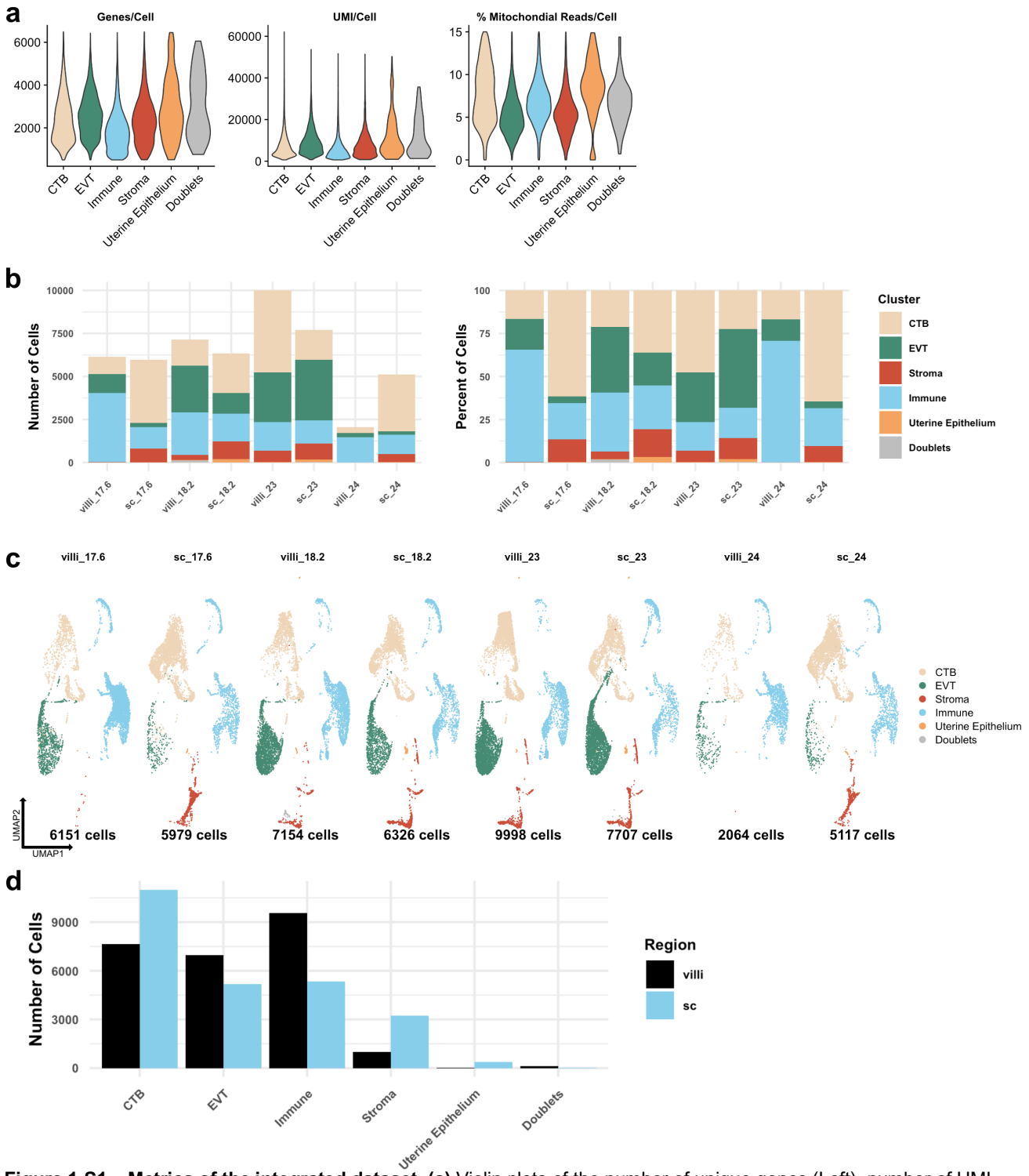

Figure 1-S1 – Metrics of the integrated dataset. (a) Violin plots of the number of unique genes (Left), number of UMI (Middle), and the percent of mitochondrial reads (Right) per cell for each broad cell type cluster. **(b)** The total number of cells (Left) and the percent of the total library (Right) in each broad cell type cluster from each placental sample are shown. **(c)** UMAP projections of the integrated dataset shown by each placental sample. Colors correspond to each broad cell type cluster in the legend at the right. The number of cells analyzed from each placental sample is listed beneath. **(d)** The number of cells in each broad cell type cluster from each placental region (VC – black; SC – blue).

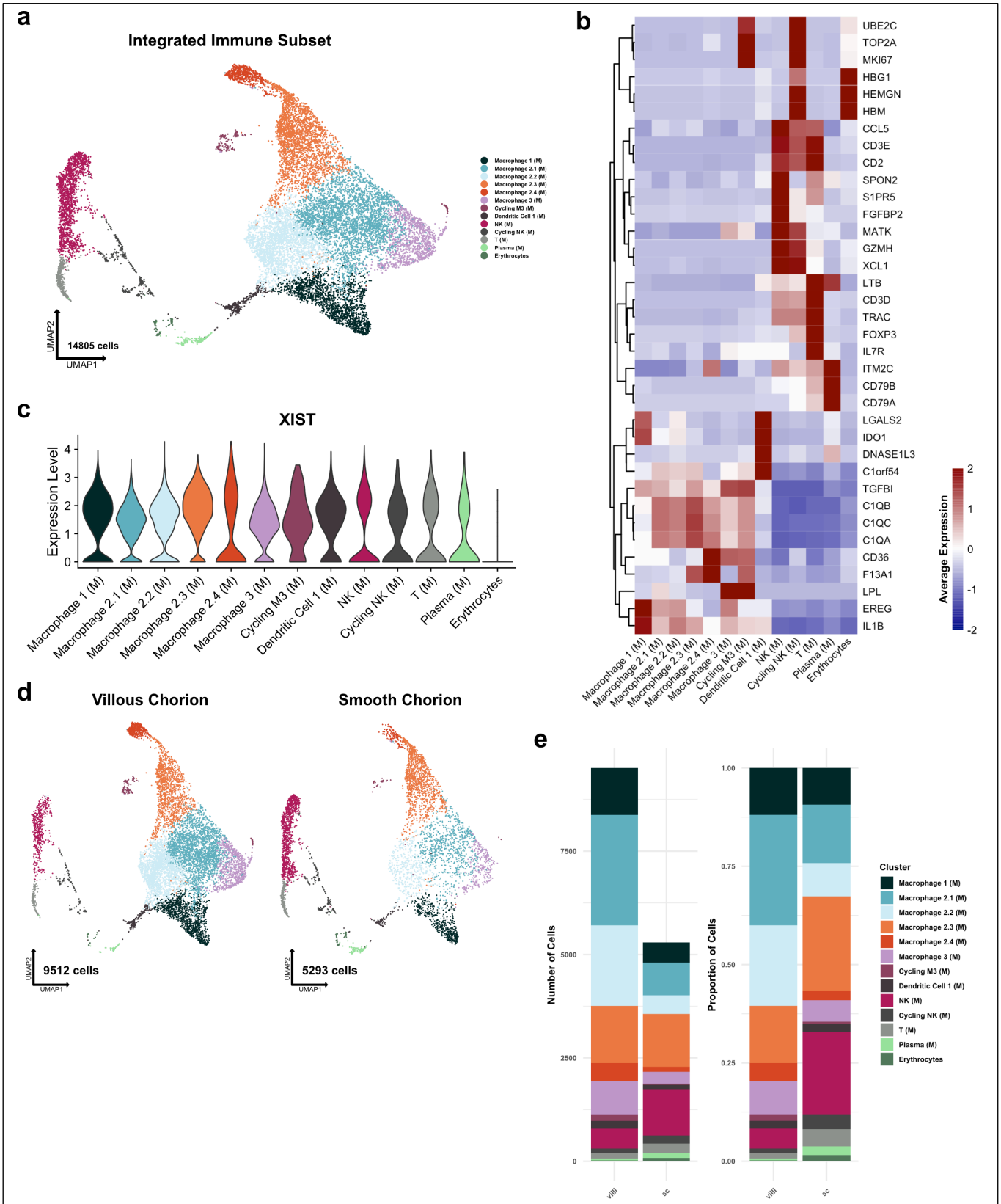

Figure 1-S2 – Metrics and markers of the immune cell subset. (a) UMAP projection of all subclustered immune cells (n=14,805). Colors correspond to the clusters in the legend at the right. **(b)** Heatmap of selected marker genes of each immune cell cluster. Expression was displayed as the scaled mean expression in the cluster. **(c)** Violin plot of XIST expression in each immune cell cluster. **(d)** UMAP projection of immune cells shown by region of origin. **(e)** Stacked bar chart of the number of cells (left) or proportion of cells (right) in each cluster by region of origin.

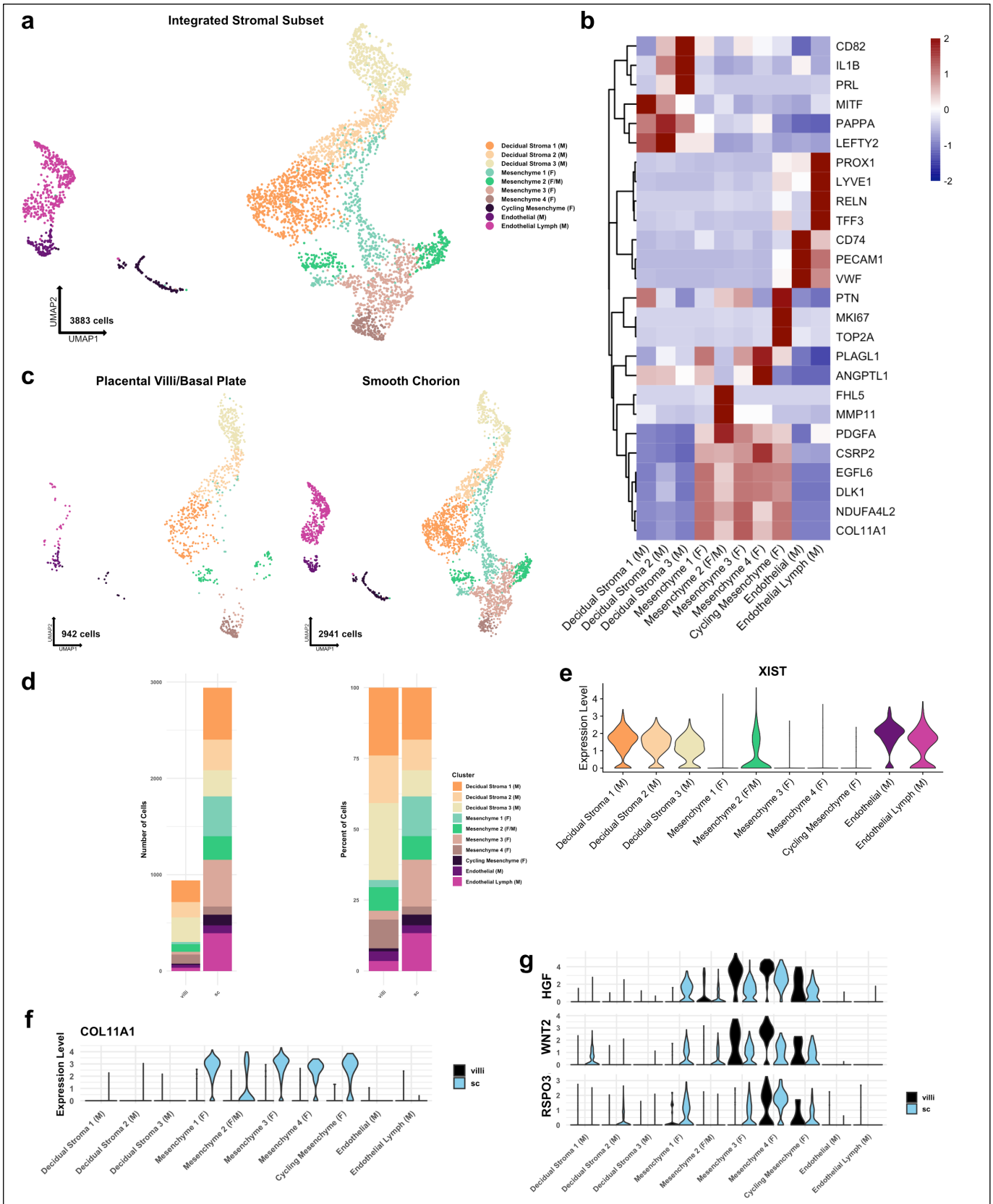

Figure 1-S3 – Metrics and markers of the stromal cell subset. (a) UMAP projection of subclustered stromal cells (n=3,883). Colors correspond to the clusters in the legend at the right. **(b)** Heatmap of selected marker genes for each stromal cell cluster. Expression was displayed as the scaled mean expression in the cluster. **(c)** UMAP projection of stromal cells shown by region of origin. **(d)** Stacked bar chart of the number of cells (left) or percent of cells (right) in each cluster by region of origin. **(e)** Violin plot of XIST expression in each stromal cell cluster. **(f)** Violin plot of COL11A1 expression in each cluster shown by each region, showing expression in only SC cells **(g)** Violin plots of HGF, WNT2, and RSPO3 expression in each cluster and shown by each region, showing expression in both VC and SC cells.

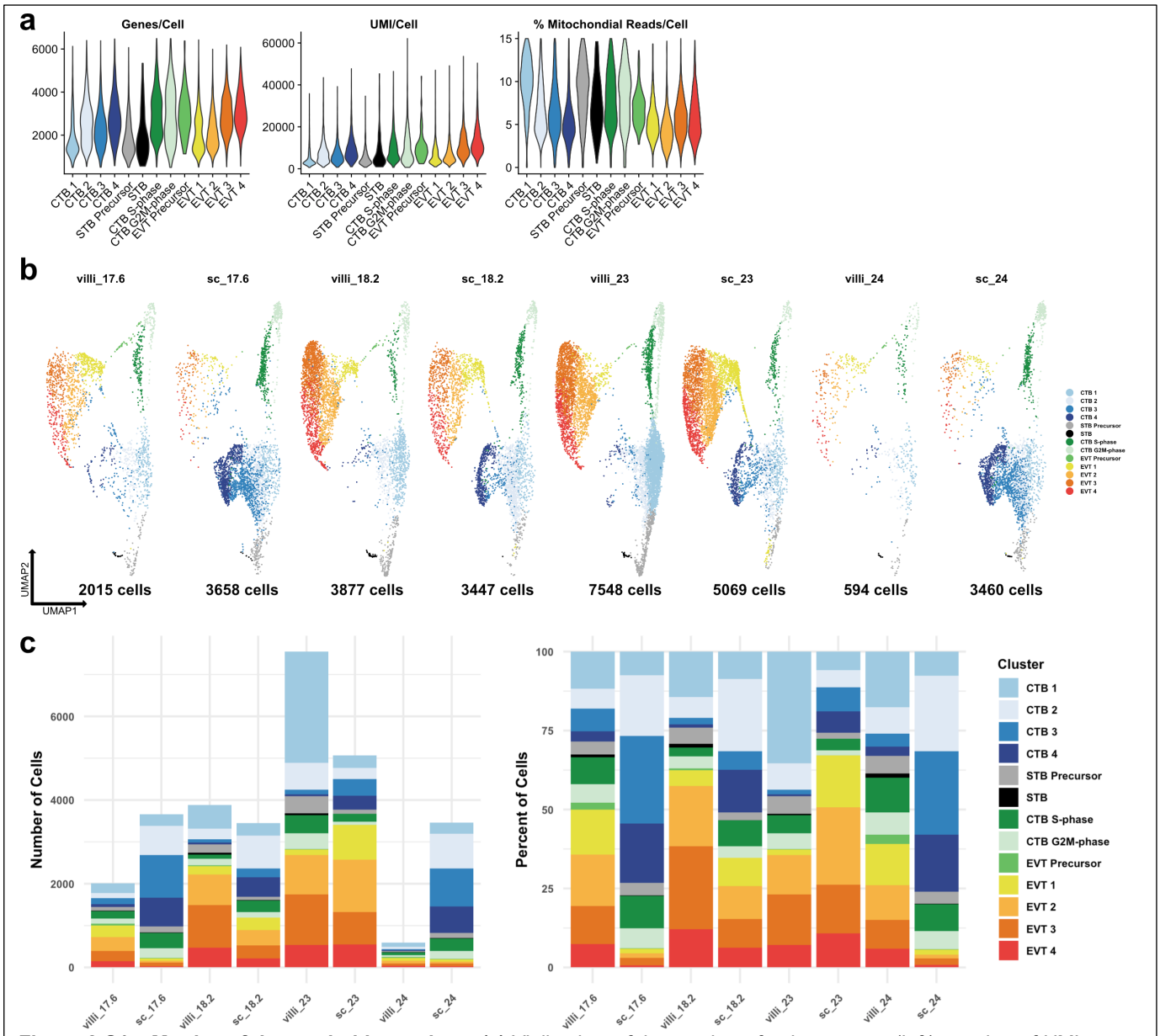

Figure 2-S1 – Metrics of the trophoblast subset. (a) Violin plots of the number of unique genes (left), number of UMI (middle), and the percent of mitochondrial reads (right) per cell for each trophoblast cluster. **(b)** UMAP projections of the trophoblast dataset shown by each placental sample. Colors correspond to each trophoblast cluster shown in the legend at the right. The number of cells analyzed from each placental sample is listed beneath. **(c)** The number of cells (left) and the percentage (right) in each trophoblast cluster from each placental sample.

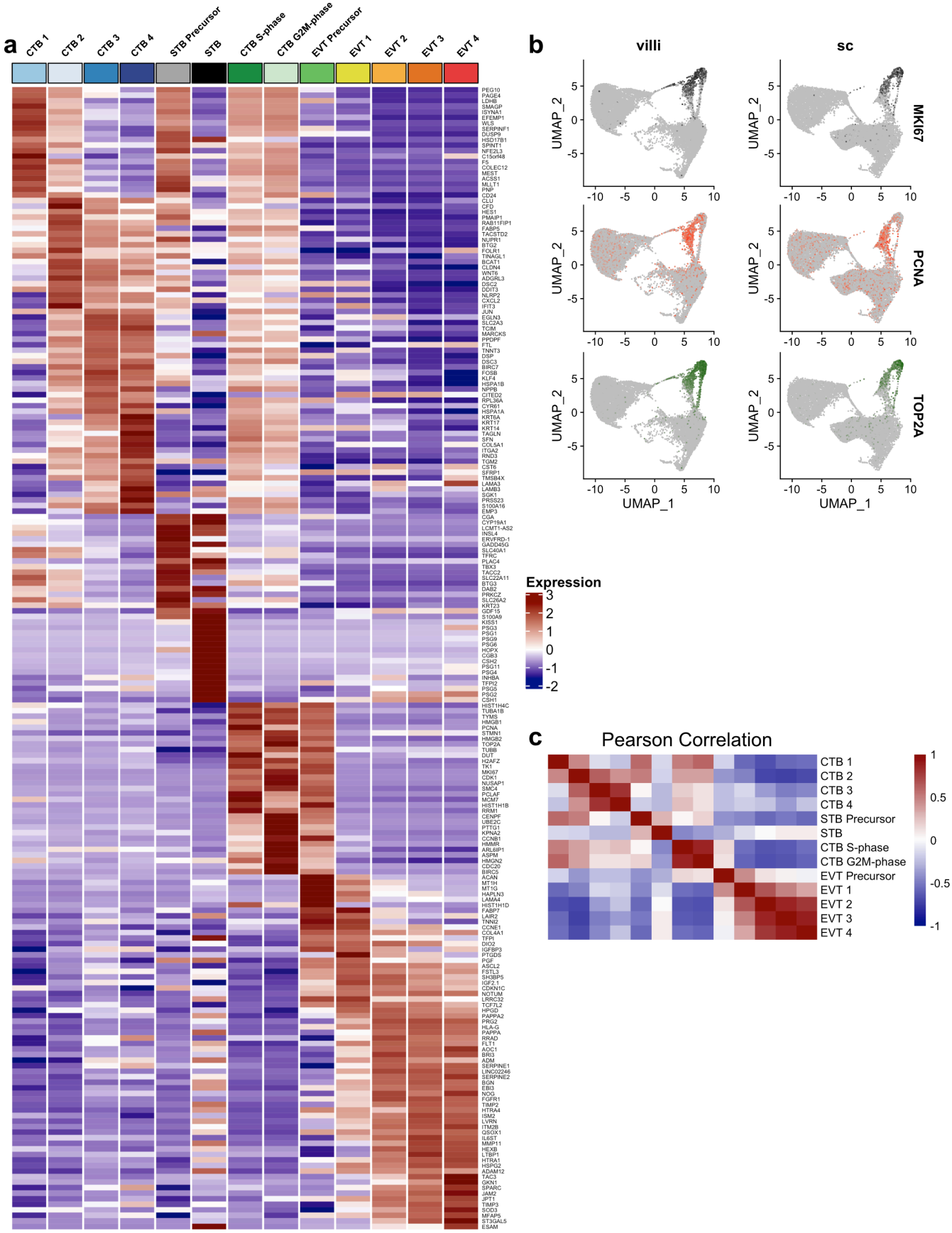

Figure 2-S2 – Metrics of the trophoblast subset. (a) Heatmap of the expression of the top 20 marker genes for each trophoblast population. **(b)** Expression of phasic transcripts MKI67 (top), PCNA (middle), and TOP2A (bottom) were projected in UMAP space. **(c)** Heatmap of the Pearson Correlation coefficients between each trophoblast population.

967
968
969

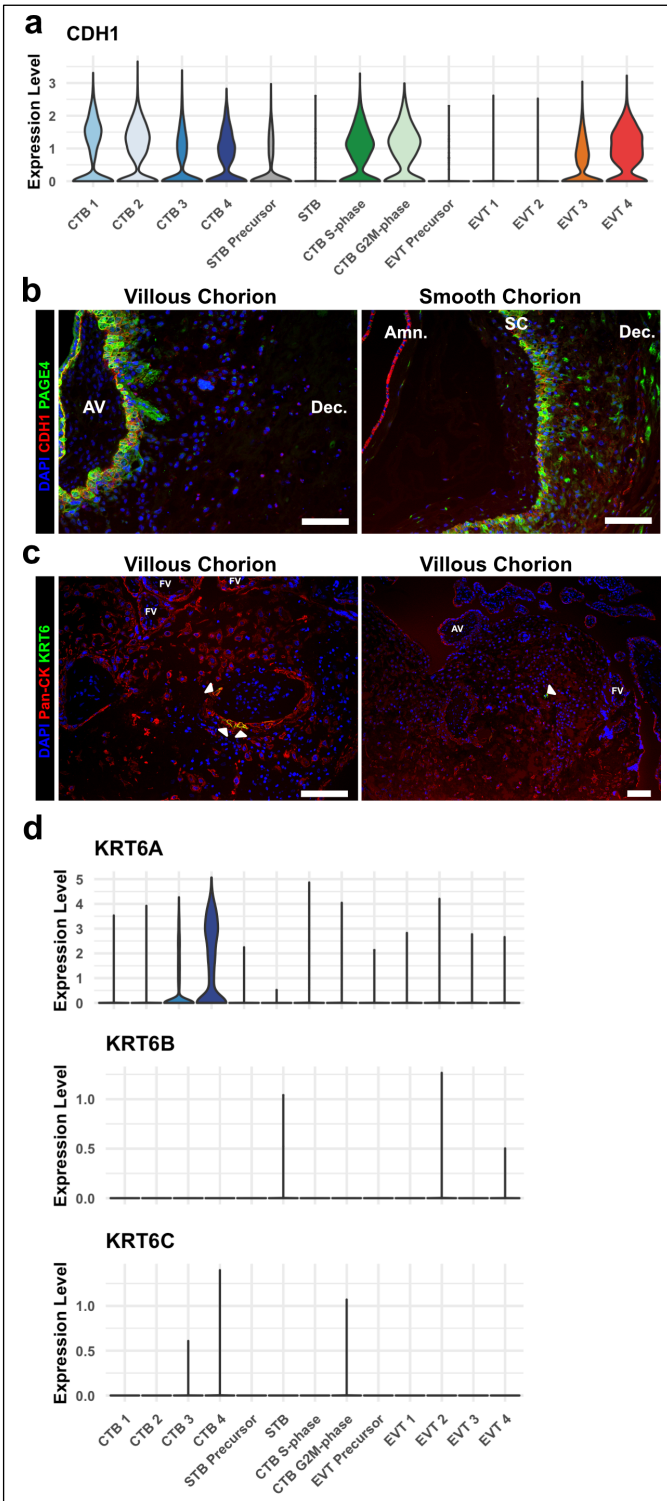

Figure 2-S3 – KRT6 expression in the VC region. (a) Violin plot of *CDH1* transcript expression across all trophoblast clusters. **(b)** Immunofluorescence co-localization of CDH1 and PAGE4 in the VC (Left) and SC (Right). **(c)** Immunofluorescence co-localization of Pan-CK (marker of all trophoblast) and KRT6 in the VC. Arrowheads denote KRT6+ cells. **(d)** Violin plots of expression of each KRT6 isoform, showing expression of only KRT6A in trophoblasts. For all images nuclei were visualized by DAPI stain; Scale bar = 100μm. Abbreviations: AV = Anchoring Villi; Amn. = Amnion; SC = Smooth Chorion epithelium; Dec. = Decidua; FV = Floating Villi.

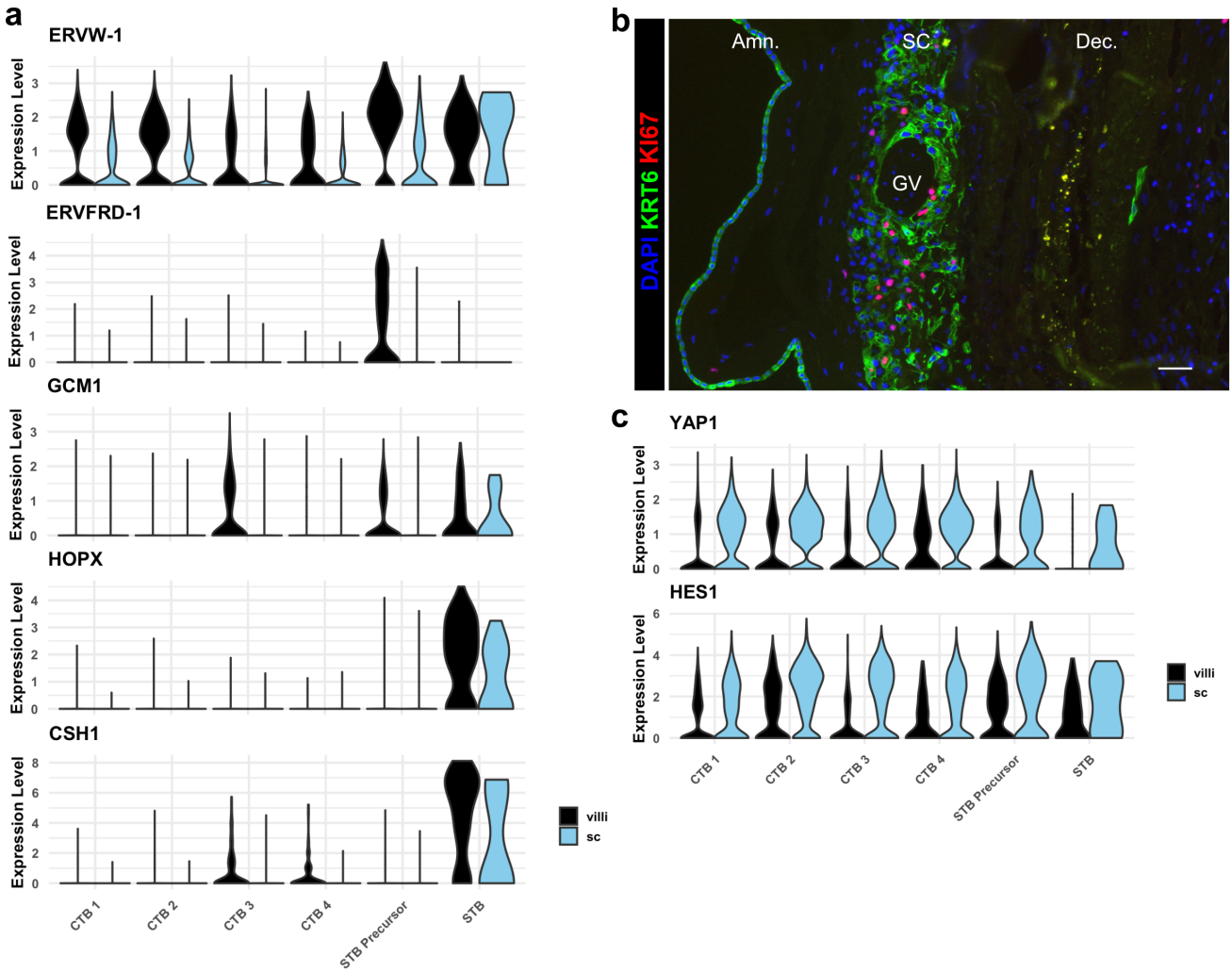

Figure 3-S1 – SC trophoblast display reduced expression of STB and increased expression of epithelial TFs. (a) Violin plots of expression of markers of STB differentiation in each trophoblast cluster shown by region, demonstrating reduced expression all markers in STB Precursor and STB clusters. **(c)** Violin plots of expression of YAP1 and HES1, demonstrating increasing expression in CTB1-4 and greater expression in the SC compared to the VC.

Figure 4-S1 – Complete CTB Gene Ontology Analysis. The unabridged Gene Ontology results from each CTB cluster, displayed as adjusted p-values. Dark red corresponds to the lowest p-values and white represents p-values greater than 0.0005. Ontology categories are organized by hierarchical clustering along the y-axis. Marker genes for each cluster were used as inputs for the analysis.

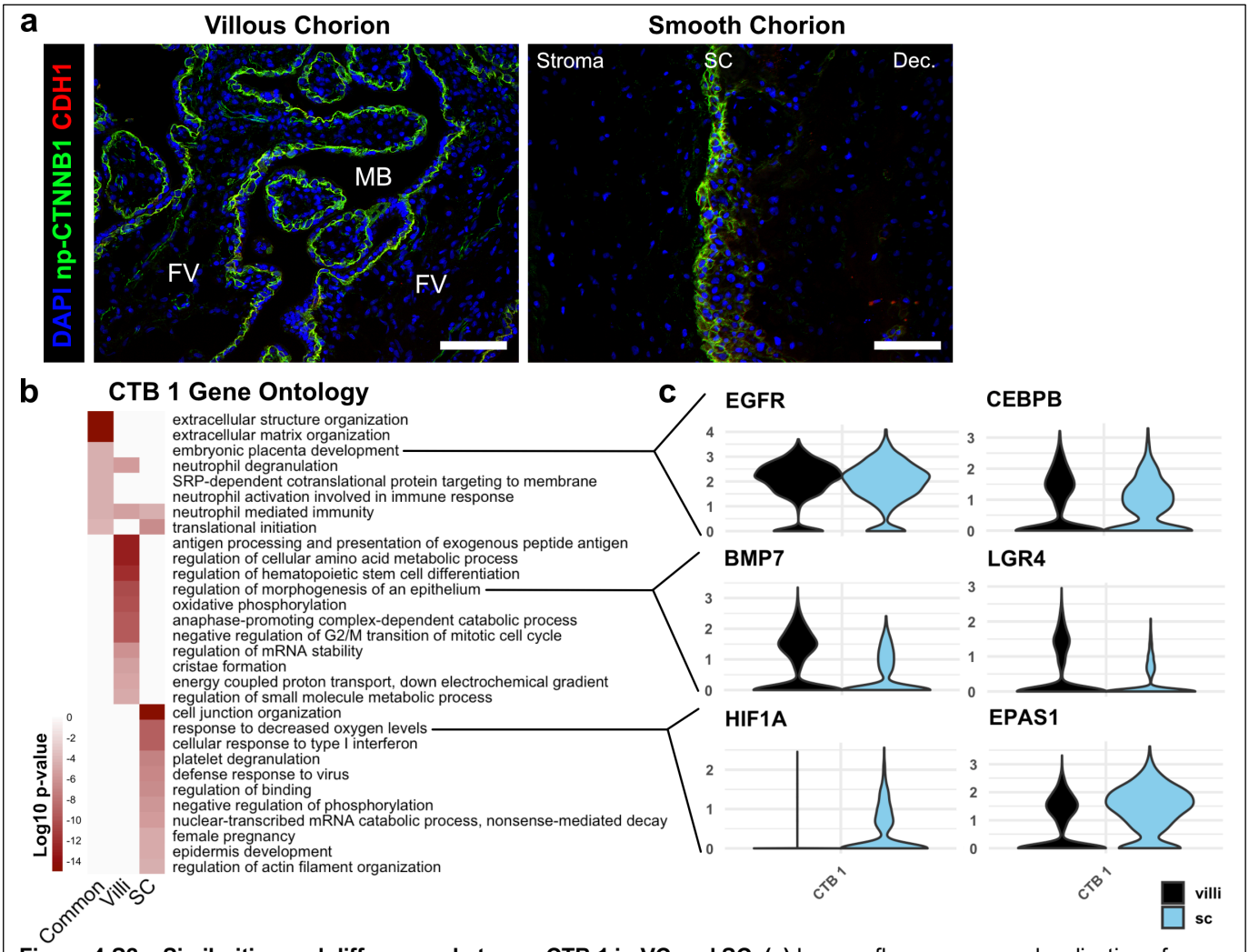

Figure 4-S2 – Similarities and differences between CTB 1 in VC and SC. (a) Immunofluorescence co-localization of CDH1 and non-phosphorylated CTNNB1 in the VC (left) and SC (right), showing identical domains of expression in both regions. For all images nuclei were visualized by DAPI stain; Scale bar = 100μm. Abbreviations: FV = Floating Villi; MB = Maternal Blood space; SC = Smooth Chorion epithelium; Dec. = Decidua. **(b)** Gene ontology analysis for CTB 1 genes common to VC and SC, genes enriched in VC, and genes enriched in SC. **(c)** Violin plots of genes within the gene ontology categories indicated in (b) for common categories (top), VC enriched categories (middle), and SC enriched categories (bottom).

979

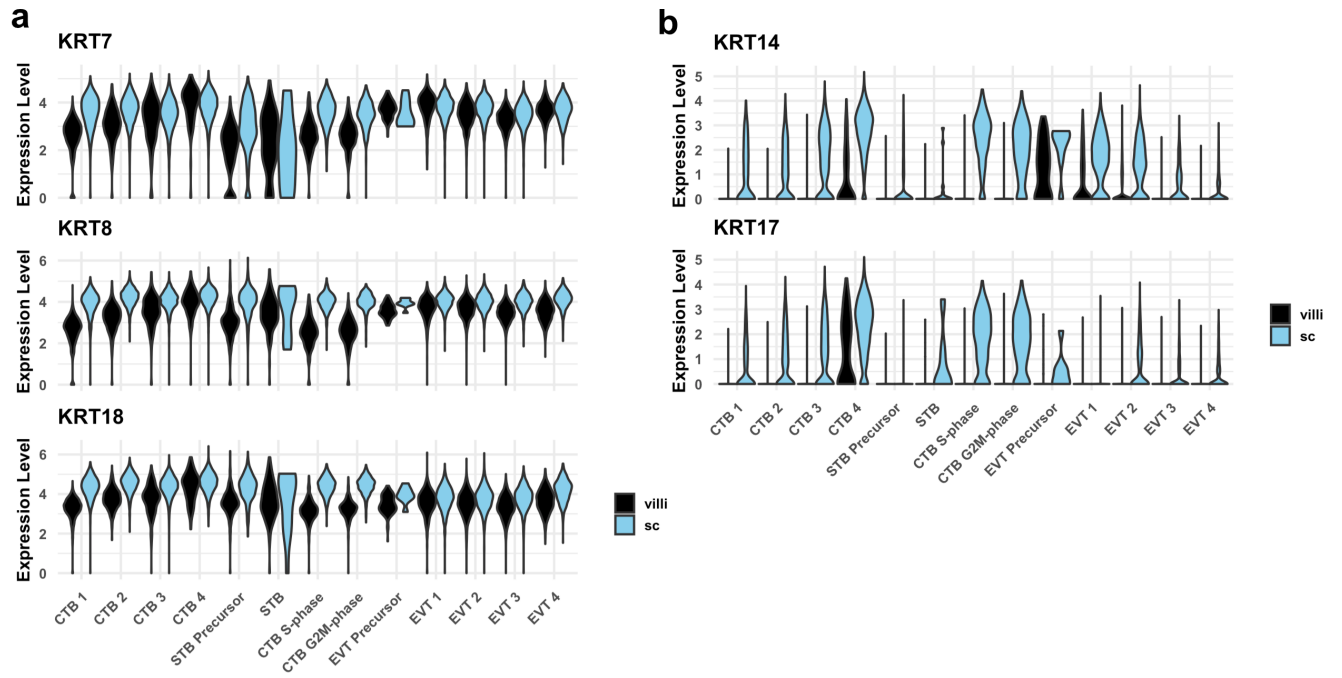

Figure 4-S3 – Cytokeratin expression in VC and SC trophoblast. (a) Violin plots of cytokeratins expressed in trophoblast in both VC and SC regions by cluster and region of origin. **(b)** Violin plots of cytokeratins expressed in SC trophoblast by cluster and region of origin.

980
981
982

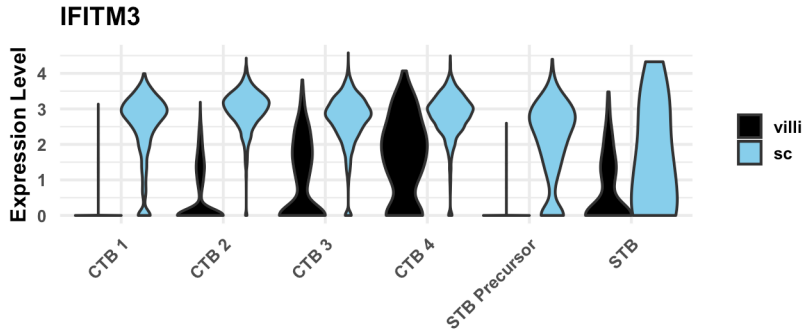

Figure 4-S4 – IFITM3 expression in CTB populations. Violin plot of IFITM3 expression in trophoblast clusters by region, showing increased expression in SC compared to VC.

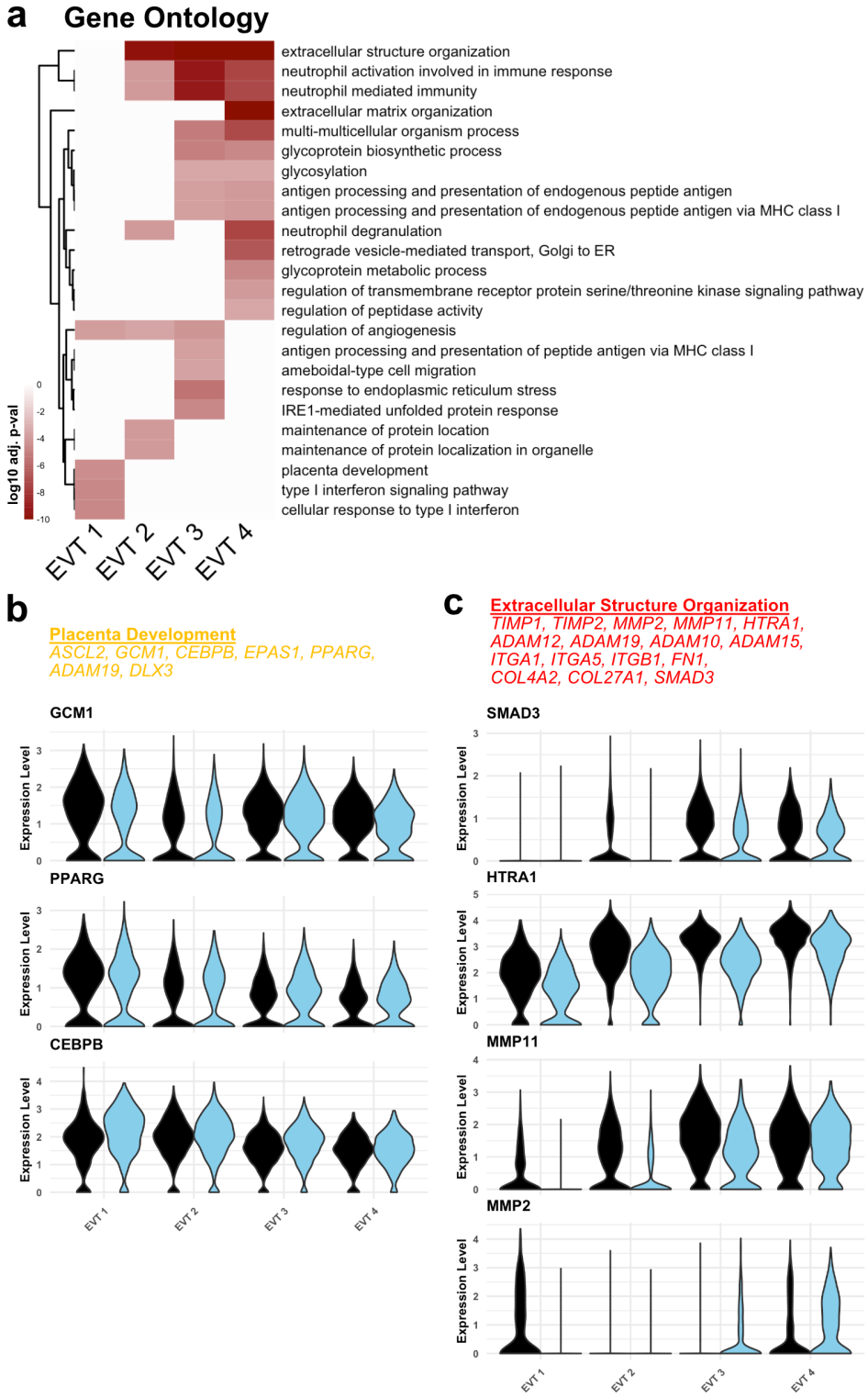

Figure 5-S1 – Functional annotation of EVT clusters. (a) Gene Ontology results from each EVT cluster displayed as adjusted p-values. Dark red corresponds to the lowest p-values and white represents p-values greater than 0.0005. Ontology categories are organized by hierarchical clustering along the y-axis. Marker genes for each cluster were used as inputs for the analysis. **(b)** Selected genes in the 'placenta development' gene ontology category (top). Violin plots of expression for selected genes in each EVT cluster by region. **(c)** Selected genes in the 'Extracellular Structure Organization' gene ontology category (top). Violin plots of expression for selected genes in each EVT cluster by region.

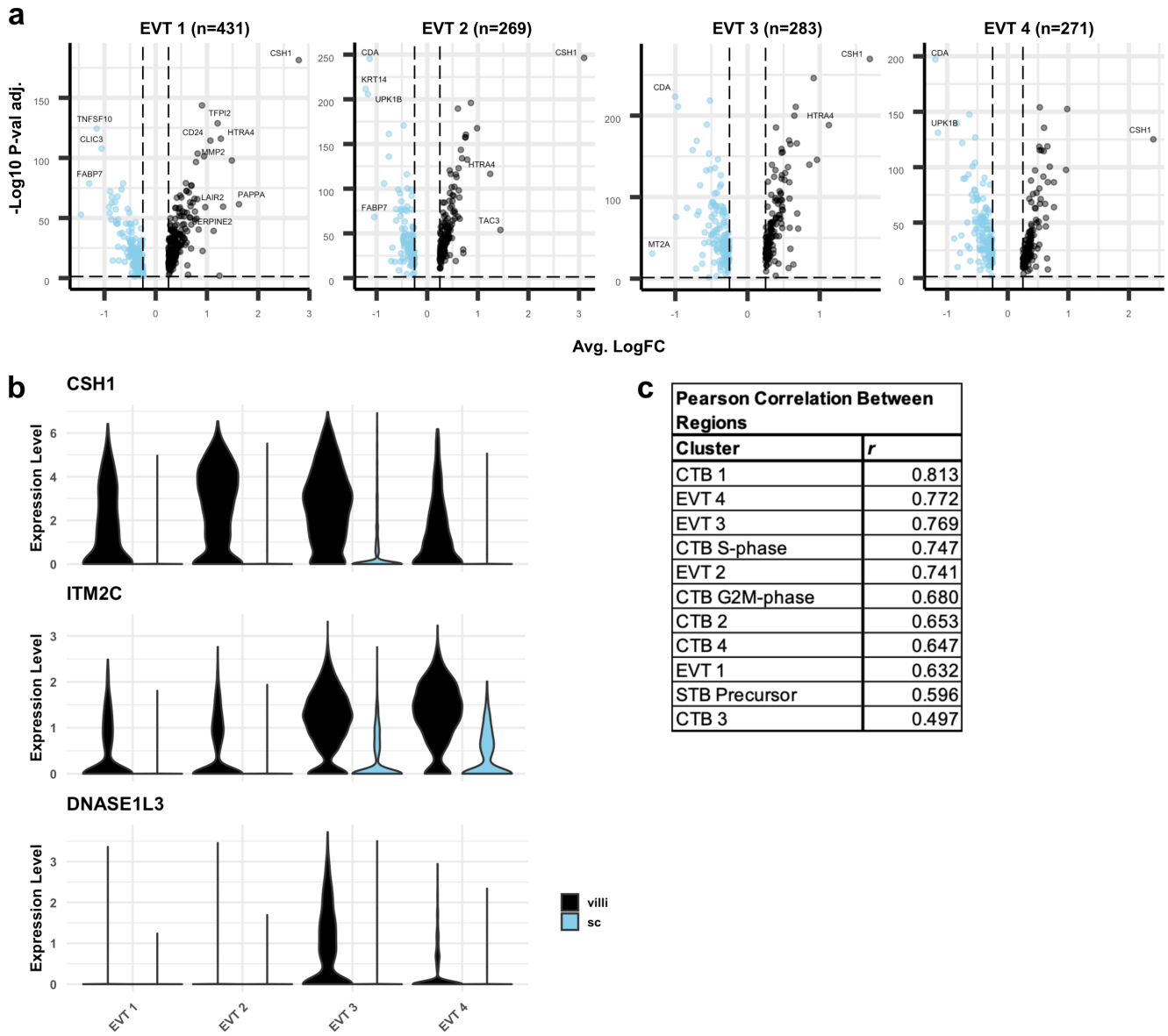

c

Pearson Correlation Between Regions	
Cluster	***r***
CTB 1	0.813
EVT 4	0.772
EVT 3	0.769
CTB S-phase	0.747
EVT 2	0.741
CTB G2M-phase	0.680
CTB 2	0.653
CTB 4	0.647
EVT 1	0.632
STB Precursor	0.596
CTB 3	0.497

Figure 5-S2 – Differential expression between EVT from VC and SC. (a) Volcano plots showing the differentially expressed genes the VC or SC for each EVT cluster. Only significantly differentially expressed genes are plotted (p-value <0.05). Genes with higher expression in VC compared to SC are shown in black. Genes with higher expression in SC compared to VC are shown in blue. Selected differentially expressed genes are labelled. **(b)** Violin plots of VC-specific genes in EVTs. **(c)** Pearson correlation coefficients between VC and SC for each cluster ranked from greatest to least similarity across regions. STB and EVT Precursor populations are excluded due to the low number of cells recovered in the SC.

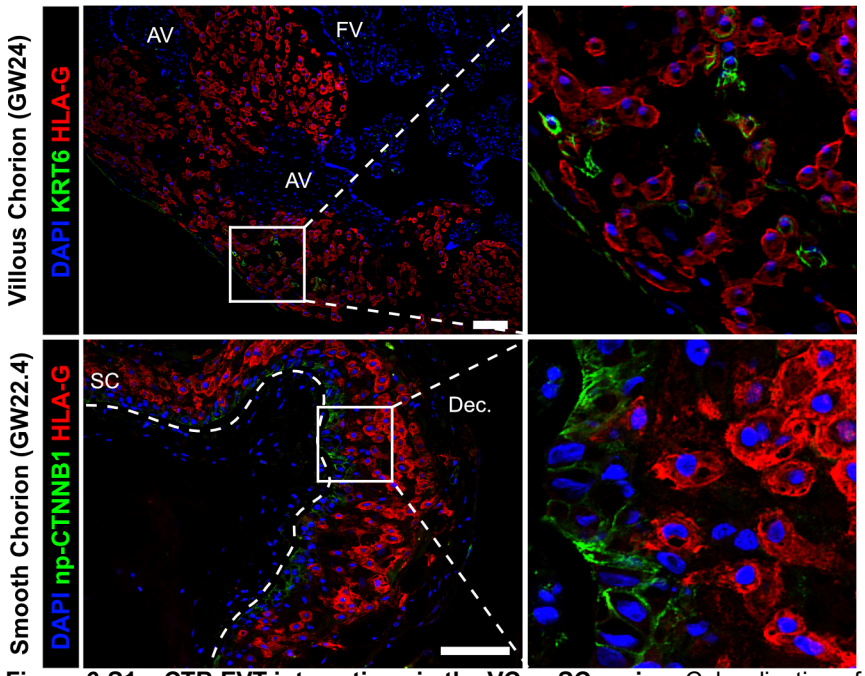

Figure 6-S1 – CTB-EVT interactions in the VC or SC region. Colocalization of KRT6 (SC-CTB marker) and HLA-G (EVT marker) showing rare KRT6+ cells in the VC (top). These cells are few and do not interact with EVT in the same manner as was observed in the SC. Co-localization of non-phosphorylated CTNNB1 (CTB 1 marker) and HLA-G (EVT marker) in the SC (Bottom). Limited interactions between these populations was observed. The basal lamina separating the fetal stroma from the SC epithelium is marked by the white dashed line. For all images nuclei were visualized by DAPI stain; Scale bar = 100μm. Abbreviations: AV = Anchoring Villi; FV = Floating Villi; SC = Smooth Chorion epithelium; Dec. = Decidua.

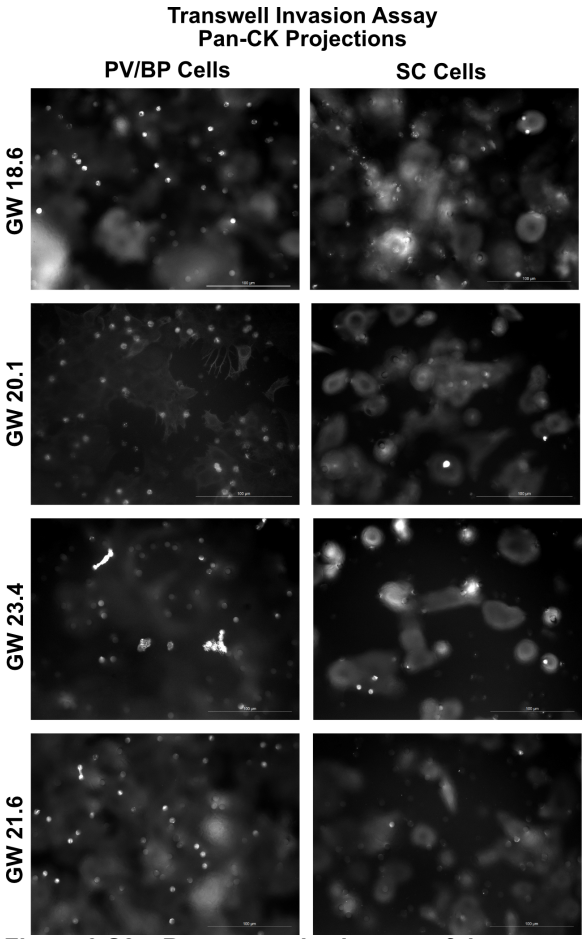

Figure 6-S2 – Representative images of the transwell invasion assay. Representative images of trophoblast projections through the transwell filter are seen a white dots. For quantification, the number of projections (white bright dots) were counted. For each sample, the median DAPI area was quantified across the transwell membrane, and then the projections multiplied by a factor to normalize for cell density. Scale bar = 100μm.

993

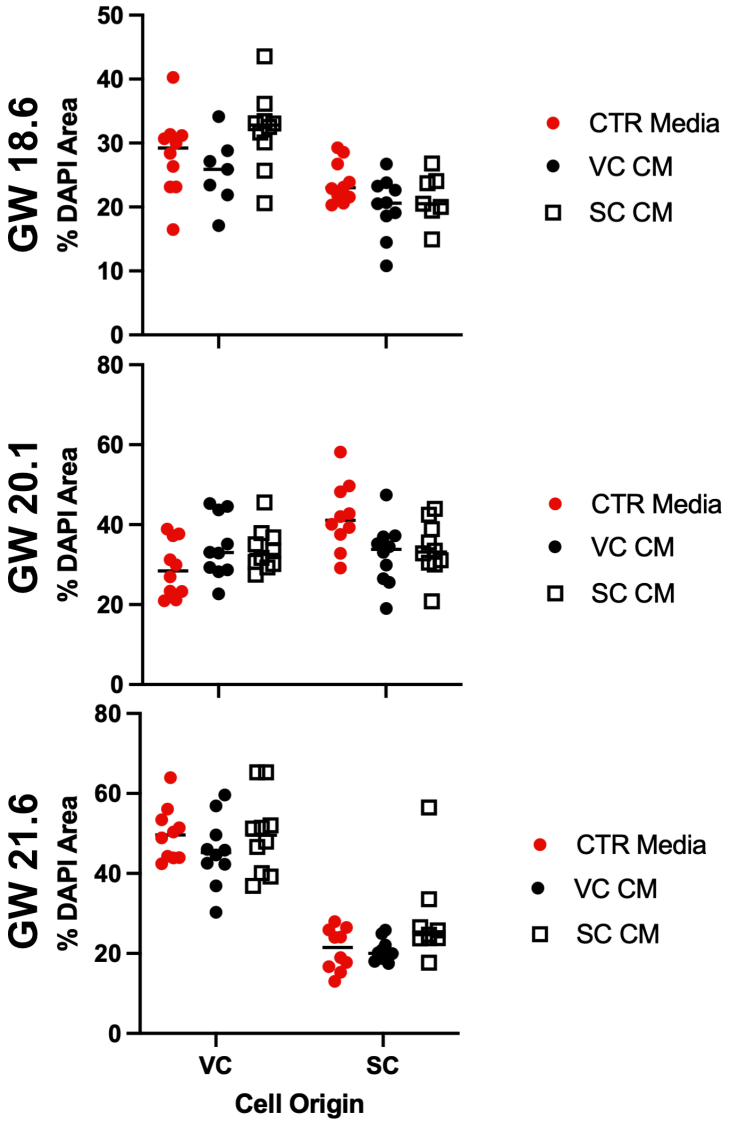

Figure 6-S3 – Cell density is not correlated with culture in conditioned media. The DAPI+ area in each field of view was quantified and plotted as a measure of cell density. Each dot represents the percent area of the field of view which stained with DAPI. Measurements from each experiment are shown and the gestational ages of the cultured cells is on the y-axis at the left. Measurements of cells treated with control media (Serum Free Media) are shown in red, VC cell conditioned media are shown in black, and SC cell conditioned media are shown in open squares.